Estimation of Supernovae Rate Densities and Demographics

Robert James Scott Airey

Department of Physics, University of Liverpool

Supervisor: Dr. Dan Perley

Submitted for the MPHYS Astrophysics Final Year Project: May 2022

Declaration of Authorship

I, Robert Airey, declare that this thesis entitled "**Estimation of Supernovae Rates and Demographics**" and the work presented in it are my own. I confirm that:

- This work was done wholly or mainly while in candidature for a research degree at this University.

- Where any part of this thesis has previously been submitted for a degree or any other qualification at this University or any other institution, this has been clearly stated.

- Where I have consulted the published work of others, this is always clearly attributed.

- Where I have quoted from the work of others, the source is always given. With the exception of such quotations, this thesis is entirely my own work.

- I have acknowledged all main sources of help.

- Where the thesis is based on work done by myself jointly with others, I have made clear exactly what was done by others and what I have contributed myself.

Signed: 

Date: **16/05/2022**

Abstract

Aims. The goal of this study was to estimate the core-collapse and Ia supernovae rate densities (SNeRDs) at low redshift (z_{avg} = 0.06) using 3.56 years worth of catalogued transient data taken by the Bright Transient Survey (BTS[1]), the largest spectroscopic supernovae survey ever conducted, which scans the entire northern sky every 2-3 days and spectroscopically analyses time varying objects brighter than 18.5 magnitudes. Secondary goals were to investigate the demographics and luminosity distributions of both core-collapse and Ia supernovae as well as the galaxies in which they were found.

Methods. Transient data from the BTS sample explorer on the 5th November 2021 was put through various justified selection cuts to leave a sample of 2214 supernovae that could be explored. An inverse volumetric rate equation and a bootstrapping technique were applied to samples of specific supernova types to yield rate density estimations out to a given absolute magnitude with 95% confidence intervals.

Results. The rate densities of core-collapse and Ia supernovae with M < -14 and M < -16.5 respectively are measured to be $1.08\pm^{0.54}_{0.24} \times 10^5 Gpc^{-3}yr^{-1}$ and $2.89\pm^{0.21}_{0.19} \times 10^4\ Gpc^{-3}yr^{-1}$ respectively. This is in good agreement with all of the previous studies conducted at low redshift. Low-luminosity host galaxies (-17 < M < -15) were found to contribute negligibly to the Ia supernova population (5.2%) in comparison to representing a larger fraction of the core-collapse supernova sample population (9.3%). The luminosity distribution of the core collapse supernova sample is extremely broad. This study also finds that the luminosity and host galaxy luminosity distributions of type II and Ib/c supernovae samples are similar supporting a claim that line-driven wind stripping does not play a key role in the loss of the hydrogen envelope from their progenitors.

Conclusions. The measured rate densities for core-collapse and Ia supernova are higher than previous values obtained in recent literature at similar redshift. The sample sizes for both core collapse and Ia supernova are the largest to date compared with previous literature. The rate density estimates should provide a local reference and comparison point for future studies.

[1] The BTS is a survey conducted by the Zwicky Transient Facility

Acronyms

SFRD – Star formation rate density, refers to the total mass of stars formed per unit volume per unit time, usually with units of $M_{\odot} Mpc^{-3} yr^{-1}$

SNe – Supernovae

CCSNe/CCSNe– Core collapse supernovae

CC – Core Collapse

SNeRD – Supernovae rate density, refers to the number of supernovae per unit per unit time, usually with units of $Gpc^{-3} yr^{-1}$

ZTF – Zwicky Transient Facility

BTS – Bright Transient Survey

IMF – Initial Mass Function

Gpc – Giga-Parsec

Df – Data frame

Contents

Chapter I: Introduction

1.1– Supernova Categorisation

Supernovae are one of the most violent and energetic events in the universe, despite the physics being unknown in the distant past, many civilisations have witnessed a supernova due to their characteristic high luminosity and they are extremely important in astrophysics and specifically in the case of core-collapse supernovae as they provide a test of our knowledge of stellar evolution as well as producing many heavy elements which will impact future star and planet formation. They are interesting events and can not only give us more information regarding the death of stars but also in terms of stellar evolution, the star formation rate, and initial mass function. The motivations for this study are discussed in **§1.4**.

Firstly, there are a few criteria that can be used to separate supernova into their several distinct types. These include progenitor, spectra lines, and light curve shape. The main focus of this paper is to discuss the results we see concerning the rates of type Ia supernova and core-collapse supernova.

The consensus model for how a type of Ia supernova occurs is through a slowly rotating carbon-oxygen white dwarf progenitor in a binary pair feeding material from its companion star which leads to the white dwarf core temperature increasing due to increases in pressure and density, consequently given that a white dwarf cannot effectively regulate this temperature as say a main sequence star can then this leads to runaway thermal reactions. It is proposed that as the Chandrasekar limit is reached, the maximum mass for a stable white dwarf is approached ($1.44M_{\odot}$) as it reaches ninety nine percent of this Chandrasekar mass, a period of convection occurs over a relatively short time period after which carbon and oxygen begin fusing into heavier elements within seconds (Röpke & Hillebrandt, 2004), this leads to a massive energy release $\approx (1-2\times10^{44}$ J) (Khokhlov, et al., 1993) is sufficient to unbind the white dwarf and the resulting shockwave can push its companion star out of the binary system. Due to this fixed critical mass that a type Ia explodes at meaning it has usually a fixed luminosity at peak when normalised and accounting for a stretch factor and can be therefore used as a standard candle with a typical blue and visual magnitude of $\boldsymbol{M_V = 19.3 \pm 0.3}$ (Hillebrandt & Niemeyer, 2000). In comparison now let us discuss core collapse supernovae and the progenitor of this.

The criterion for a core collapse supernova is that its progenitor must have a zero-age main sequence mass greater than eight but no more than 40-50 solar masses (Gilmore, 2004). This type of progenitor is fusing heavier and heavier elements with increasing temperatures and pressures until it reaches a nickel-

iron core and given these two elements have the highest binding energy per nucleon (Fewell, 1995) of all the elements then this renders the core inert and there isn't sufficient outwards pressure from fusion to balance out gravity and give hydrostatic equilibrium across the star thus the core contracts and this contraction is largely halted by an electron degeneracy pressure, however once the core reaches and exceeds a mass of the previously defined Chandrasekar limit, the inner core implodes leaving the outer core to collapse and this sudden compression heats the core to billions of kelvin which thermonuclearly leads to the production of neutrons and neutrinos via a reverse beta decay. Due to the production of neutrons this leads to a neutron degeneracy pressure to hold up the inner core's collapse and thus the imploding shockwave is rebounded by these dense neutrons and disrupts and pushes the stellar material outward and thus this is the supernova explosion. The energy from this shock dissociates heavy elements within the core. This dissipates the energy of the shock which can stall the explosion within the outer core (Fryer & New, 2003). Two neutrino production mechanisms convert the gravitational potential energy of the collapse into a ten-second neutrino burst given that the core collapse is so dense that only neutrinos can penetrate outwards, releasing about 10^{46} J (Barwick & Beacom, 2004), The shockwave also allows a brief period of time where the temperature is sufficiently high enough to fuse heavier elements than iron. (NASA, 2011) There are also two other types of core collapse supernovae to note. Types Ib and Ic which are stripped core collapse supernova due to their progenitors losing their outer envelopes of hydrogen (Ib) and hydrogen/helium (Ic) because of strong stellar winds. However, their core collapse mechanism is the same as a type II as described previously.

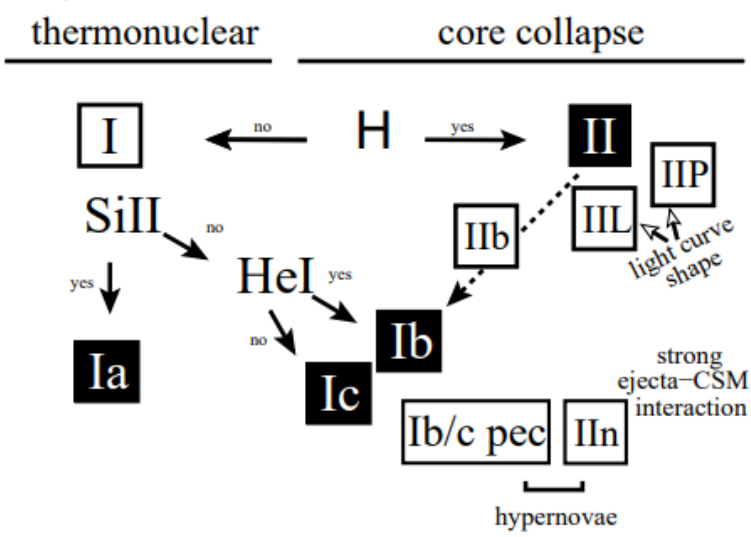

Figure 1 - A useful diagram relating the spectral and light curve differences between supernovae classes as well as the underlying mechanisms. The main criterion to distinguish between supernovae comes spectroscopically *(Turatto, 2003)*

From this diagram, the types of supernovae are well defined spectroscopically. For example, a type I and type II supernovae are defined from whether they show significant hydrogen lines in their spectra and again moving downwards, types Ib and Ic are separated from whether they show strong He-1 lines.

1.2 –ZTF and BTS

In this short subsection, the Zwicky transient facility and bright transient survey are introduced to provide a brief background as to how this facility collects and provides data for this study.

The Zwicky Transient Facility is a public-private partnership tasked with studying the optical night sky particularly in the r and g photometric bands. The ZTF aims to scan the entire northern sky about every 2-3 days using an extreme wide field of view camera in particular a ccd camera which utilises the entire focal plane of approximately forty-seven square degrees of the P48 Palomar telescope. This large area survey allows for the study of wide range of time-domain astrophysical phenomena whether that is near earth asteroids or supernovae. The latter being the topic of this study. The ZTF bright transient survey is a large spectroscopic survey focused on supernovae. This survey started in June 2018 and since then has been surveying the entire northern sky (see Figure 2) every 2-3 nights in the r and g filter bands and has been acquiring spectra for objects brighter than 18.5 magnitudes. In a dubbed phase I lasting from the beginning of the survey to 2020, the BTS catalogued and confirmed around four thousand SNe. They expect that over phase II (until 2024) that this number will increase to around 10,000. The BTS catalogues of course SNe but also other exotic transients too such as tidal disruption events (TDE's) and novae for example. They have provided classifications for over five thousand spectroscopically verified objects. It is important to note that the ZTF and subsequently the BTS is sensitive at low redshift.

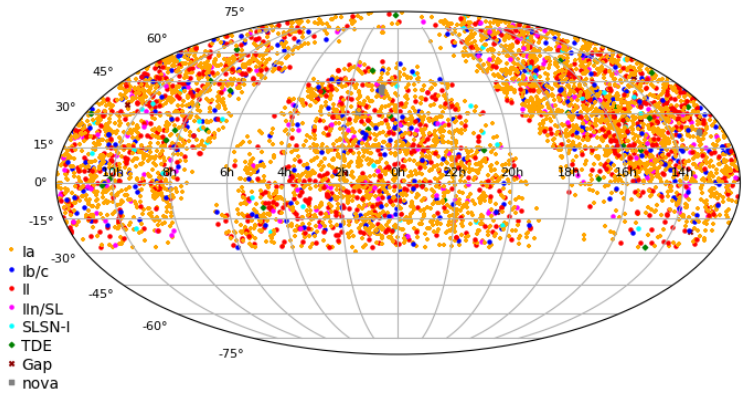

Figure 2 – An example of a sky map taken from the BTS website. Showing the relative locations on the sky of various transients with respect to the celestial sphere. As mentioned, the BTS scans the entire northern sky every 2-3 nights which leads to this diagram here. Which shows a very well catalogued northern hemisphere. (Perley, 2022)

The data for this study was taken from the BTS sample explorer in CSV format on the 5th November 2021. The BTS sample explorer being a useful tool to display and explore the ZTF Bright Transient Survey sample. It is automatically updated every few hours. The sample taken from the BTS sampler explorer will be discussed more in **Chapter III** and a link to the BTS sampler explorer can be found in the appendix of this document.

1.3 – Bootstrapping Theory

In this subsection, the technique behind bootstrapping, the advantages and disadvantages of bootstrapping and the need for a bootstrapping technique will be discussed and applied to the context of this study.

Bootstrapping is a statistical tool used to derive estimates for quantities such as standard errors and confidence intervals. It can be thought of as a resampling method as it involves using random sampling with replacement to make these estimations. In the context of this study, a bootstrapping technique is used to derive 95% confidence intervals for given supernovae rate densities. Bootstrapping techniques have been recommended more frequently as computing power has increased, with the idea that increasing the number of samples cannot increase the amount of information in the original data however it can reduce random sampling errors. In particular even a sample size as small as fifty will lead to good standard error estimates. In a paper by Ader et al, they recommend that a bootstrap be applied in certain situations such as: when the theoretical distribution of a statistic of interest is complicated or unknown. Or in other words in situations where there is no standard or normal theory to describe the statistics of a population or sample. In a situation where there is a small or insufficient sample size to infer derived statistics. If there is a reasonable defined distribution in the sample, then a bootstrap can account for a sample that may not be entirely representative of a larger population. When a power calculation has to be performed with a given small sample associated with them. Can get the idea of the variation of a statistic such as a standard deviation which is often required in power calculations by performing a bootstrap on a small initial data sample.

A bootstrap is advantageous as it is very simple to derive standard errors and confidence intervals as is shown in **§3.3**. Despite the simplicity, a bootstrap can be applied in much more complex regimes such as samples divided into multiple strata with a given number of observations for each. Another advantage is that a bootstrap can assess the stability of results and bootstrapping is also asymptotically more accurate than standard intervals taken from using other sample statistics. Finally, another relevant advantage to

this study in theory is the fact that bootstrapping removes the need for repeating observations to get another data sample.

However, there are disadvantages associated with bootstrapping too as with any method. If bootstrapping is ignorantly used without form or reason, it can yield invalid results and consequently inconsistencies. Another disadvantage of bootstrapping and in particular as shown in ***Table 1***, it can be very time consuming as there are few autonomous methods in programming that can carry a bootstrap out, although of course the time estimates in ***Table 1*** depend heavily on computing power and the operation being performed. Athreya also showed that if a naive bootstrap is performed on a sample that lacks a finite variance, then the bootstrap will not converge on the statistic that is being derived. Confidence intervals derived from a Monte Carlo of a bootstrap can be misleading.

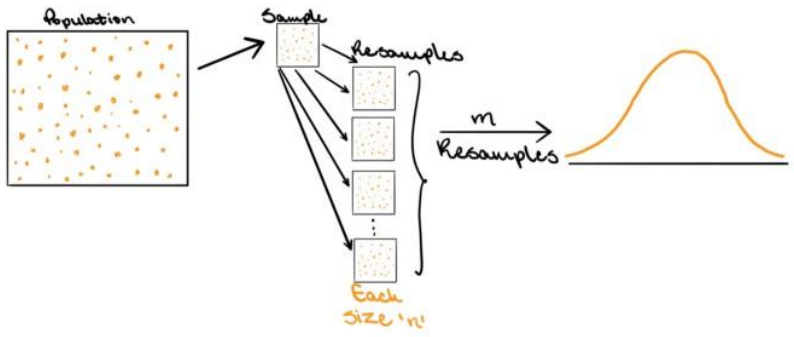

Figure 3 – Simplistic overview of a bootstrapping technique. A sample is taken and resampled multiple times where the samples and resampled datasets are of the same size. This can there be used to show the distribution of a statistic of a larger population from which a sample was taken from. *(Joseph, 2020)*

Figure 3 shows the general idea for a bootstrap. A sample is taken of a larger population and resampled with replacement multiple times, but the key distinction is that both sample and resamples are of the same size or are arrays of the same length. This resampling allows for the distribution of a statistic of a larger population to be known as is shown by the orange curve in ***Figure 3***.

1.4 - Motivations for this study

Firstly, the motivation for studying the demographics of supernovae comes from the ever-growing need to catalogue and quantify the populations of these supernovae, how many and how bright? Therefore, by seeing how many supernovae are found and consequently the photometry associated with that allows for a greater understanding of how often we should expect to find these events and typically what luminosity

we should expect them to have, which in turn will allow more fine-tuning in the sensitivity of observational facilities or telescopes to certain magnitudes for more direct study of SNe.

In this study, supernovae rates are also estimated given the host galaxy they occur in by seeing the distribution of SNe and SNeRDs across host galaxy luminosities, this is motivated by the interest in seeing how supernovae rates change as a function of the host galaxy luminosities, are supernovae more common at certain galactic luminosities? This would also allow for further discourse surrounding the relation of progenitors to the galaxy properties they lie within.

Another motivation is related in particular to core collapse supernovae. Again, as mentioned in **§1.1**, CCSNe have progenitors with a fairly well defined upper and lower mass limits, this means that the Salpeter initial mass function can be directly implicated into this study. Therefore, by taking star formation rate densities found in literature and converting these to supernovae rate densities using **Equation 1** defined in **§2.2**, the star formation rate can be directly compared to the rate density of CCSNe in this study and a consensus of how many of these SFRDs agree or disagree and why. (Horiuchi, et al., 2011) established a SNe rate problem whereby the massive star formation rate was twice as large as the measured CCSNe rate, this paper aims to give a deeper insight into whether this supernovae rate problem is still apparent.

Chapter II: Establishing Methodology from Literature

In this section, the inverse volumetric rate equation and converting from SFRDs to SNeRDs is established from the literature. How previous studies have dealt with incompleteness within their samples is also discussed.

2.1 – Sample Completeness

The completeness of a sample describes how complete a sample is with regard to a certain variable. For example, the BTS is about 95% complete to classifying SNe brighter than 18.5 magnitudes. Many different studies have had to account for sample incompleteness in regard to supernovae studies and rate density estimations.

2.1.1 - Nearby Supernova Rates from the Lick Observatory Supernova Search. II. The Observed Luminosity Functions and Fractions of Supernovae in a Complete Sample

The first study by Li et al (2011) was tasked in using the Lick observatory to estimate local supernovae rates and the fractions of SNe in their sample.

First, they calculated a control time for each supernovae based on a chi squared light curve fitting technique based on the photometry they had collected during the observation period. They defined the completeness to a particular SNe as the sum of the control time of that particular SNe for all galaxies within that distance divided by the sum of the season time for these galaxies. To correct a supernova type to 100% completeness within a cut-off distance of the luminosity functions, they took the reciprocal of the completeness a corrected number for the SNe. They find that type Ia SNe have a larger completeness due to their extremely high luminosity at peak and that the majority of completeness is greater than 80% for a cut off distance of 60 Mpc. Some SNe have low completeness due to extremely faint luminosities (usually an issue with CCSNe) and reddening effects.

To make the sample more compete they suggested that adding follow up samples with unknown completeness's or biases could be effective however this would require larger corrections to compensate, or they suggest using a catalogue of supernovae, which in fact is what the BTS can be referred to as.

With regards to luminosity functions, some luminosity functions are taken as an average luminosity with a gaussian spread whilst others take luminosity functions as they are observed, and they may also be taken as the intrinsic luminosity functions with extinction corrections applied.

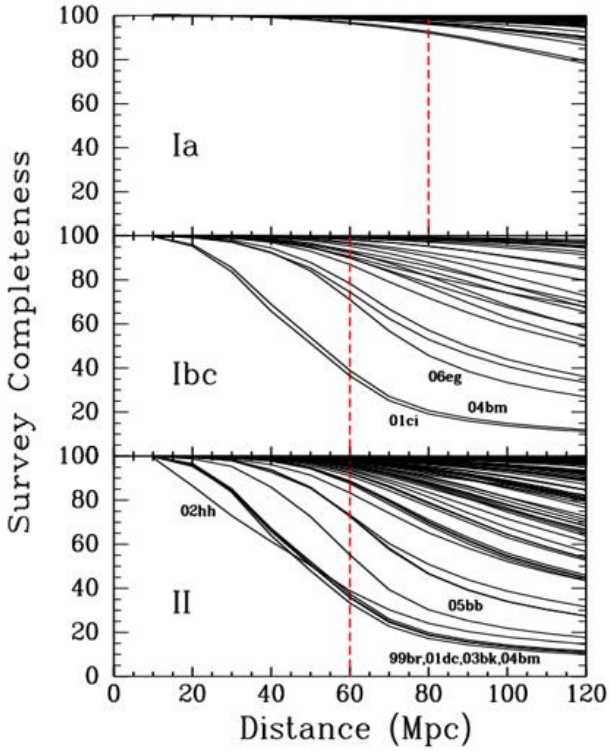

Figure 4 – The completeness of each SNe type in the luminosity functions in the survey. The red dashed line represents the cut-off distance at which the luminosity functions are constructed. The top panel is the sample corresponding to type Ia SNe, the middle panel representing type Ibc SNe and the bottom panel representing type II SNe. (Li, et al., 2011)

We see in ***Figure 4***, the sample completeness as a functions of cut-off distance from which the luminosity functions are calculated. They find that type Ia SNe have a larger completeness due to their extremely high luminosity at peak and that the majority of completeness is greater than 80% for a cut off distance of 60 Mpc. Some SNe have low completeness due to extremely faint luminosities (usually an issue with CCSNe) and reddening effects.

2.1.2 – The Cosmic Core-Collapse Supernova Rate Does Not Match the Massive Star Formation Rate

In this study by Horiuchi et al (2011), they found that catalogued low luminosity SNeRD's falls with distance and this a sign of incompleteness. Any significant decrease in catalogued SNeRD's points out a lack of completeness for SNe discoveries at that distance. Given that this is the case they suggest that all catalogued SNeRD's be considered as lower limits given that they are derived from simple counting of incomplete SNe discoveries. For particularly dim CCSNe, it is not desired to go out to further distances due to the lack of detectable CCSNe, the sample would become incomplete. To correct for this, they chose a local distance of 10 Mpc which yielded a sufficient number of low luminosity CCSNe to study.

The majority of SNe searches they made in this local volume had limiting magnitudes of eighteen which corresponds to an absolute magnitude of approximately -12 magnitudes, therefore they conclude that their local sample is only limited by the incompleteness by the galaxies that have been observed which explains why they find the dim fraction of CCSNe is smaller at larger distances (30-40 Mpc).

2.1.3 – Completeness with Regard to ZTF & the BTS

The advantage of using SNe data from the ZTF and BTS in this study is that incompleteness issues are much easier to deal with. The ZTF's upper apparent magnitude detection limit is twenty-one magnitudes and at 19 magnitudes it is almost 100% complete to detecting SNe. The BTS is designed to be about 95% complete to classifying SNe brighter than 18.5 magnitudes.

Secondly the BTS detects so many objects that transients which have poor light curves can be thrown out of a sample therefore leaving only SNe with good light curves within without applying any biases. This is done with purity and quality cuts which was a key part of the selection cuts made in this study (see **§3.1)**

2.2 – Inverse Volumetric Rate Equation

This sub-section is to briefly establish how an inverse volumetric rate equation in the study conducted by Perley et al (2020). This is a key paper to establish an equation that is very key to this study and the methodology that can be found in **Chapter III.** In this study, they were looking to estimate supernovae rate densities as well as SNe demographics using data from the ZTF and the BTS. So, there are similarities between the study presented here and Perley et al which means that it is appropriate to apply certain aspects of the methodology. The equation below is what they use to infer and estimate their SNe rates.

$$R = \frac{1}{T}\sum_{i=1}^{N} \frac{1}{\left(\frac{4}{3}\pi D_{i,max}^{3}\right) f_{sky} f_{cl,i} f_{ext} f_{r}}$$ **Equation [1]** (Perley, et al., 2020)

First let us consider each component of ***Equation [1]*** as well as the motivation for using such an approach like this:

- T represents the total survey time, this was 3.56 years (1300 days)
- $\frac{4}{3}\pi D_{max,i}^{3}$ represents the limiting volume out to which the ith transient can still be detected above m_{lim} at peak light in the absence of extinction, given its peak absolute magnitude M_i. $m_{lim} = 18.5$ in this case. The calculation to get to $\frac{4}{3}\pi D_{max,i}^{3}$ is provided within the appendix.
- $f_{sky} f_{cl,i} f_{ext} f_{rec}$ represents the loss factors applied to account for the loss of survey volume and for the gain of transients that occurred outside the survey duration but were detected on their rise or decline to/from peak. The values they take in this study and more information on their calculation can be found in **§3.2**

In the study conducted by Perley et al (2020), they of course assume slightly different loss factors and apply a k correction (dependence on redshift) however the subsequent methodology and statistical uncertainty calculations are similar if different from in **§3.2** and **§3.3.** The results of the study conducted by Perley et al can be found in ***Table 2*** and ***Table 3*** in **Chapter IV**

2.3 – Star Formation Rate Densities and Salpeter IMF

The IMF is an important quantity in astronomy as it describes the initial distribution of masses of a stellar population through an empirical function. The properties of many stars such as lifetime, luminosity and evolution are related through their initial mass.

The IMF is often given as a power law and in relation to this study and the subsequent conversion of SFRDs into SNeRDs involves a form of the IMF denoted as the Salpeter IMF (see appendix for the specific form). This IMF has a power index of -2.35 and showed that the number of stars in a mass range decreases rapidly with increasing mass.

The IMF is important in the conversion mentioned before as given that CCSNe have a fairly well-defined mass range, often quoted as between 8 and 50 solar masses. Therefore, the IMF can be combined with a time dependent density function as it reveals how many CCSNe should form in a given volume.

In the study conducted by Horiuchi et al (2011), they assume a dust corrected star formation compilation and a smoothed power law which is the time dependent density function (see appendix). This was an appropriate over a range of redshift and was applicable with a Salpeter IMF.

$$R_{SN} = 10^9 \rho_*(z) \frac{\int_{M_l}^{M_u} M^{-2.35} dM}{\int_{0.1}^{100} M^{-1.35} dM} \quad \textbf{Equation [2]}$$

Equation [2] is a slightly modified form of equation two found in Horiuchi et al (2011). It can be thought of as a conversion formula, going from an SFRD to a SNeRD. A breakdown of each term explains the logic of using this equation. The factor of 10^9 is needed for the sole purpose of comparison as usually SFRD are given in units of $M_\odot\ yr^{-1}Mpc^{-3}$ however the SNeRD's which are stated in this paper are given in $yr^{-1}Gpc^{-3}$, the factor of 10^9 is purely to change the volume unit.

The factor $\dot{\rho}_*$ is the time derivative of a redshift dependent density function and the integrals are Salpeter initial mass functions. The fraction of Salpeter IMF's can be thought of as an efficiency of forming CCSNe.

Chapter III: Methodology

This analysis described in this chapter was performed in python and specifically involved PANDAS to create data-frames. These were used in defined functions that usually contained for loops and plotting routines to produce rate curves and the subsequent 95% confidence intervals associated with them that will be seen in **Chapter IV**.

3.1 Sample & Selection Cuts

As mentioned in **§1.2**, the BTS survey (see **Chapter VIII** for link) provided the data sample for this analysis. Data was taken as CSV on the 5th November 2021 and contained transient data over a 1300-day

period (3.56 years). This sample initially contained 8569 transients of diverse types. As you would expect this was a very raw sample of data and various selection cuts needed to be made in order for it to be appropriate for estimating SNe rates. Firstly, the CSV file was loaded into a PANDAS data-frame so that the following cuts could be applied. The first cut was to drop all transients which contained incomplete information particularly if that information was the luminosity and apparent magnitude at peak. This was justified as the photometric data was the most important for estimating the supernova rates, in fact it was a key component in determining the volumetric rate as seen in **§3.2** therefore having incomplete data was not useful. The second cut was to keep all transients that had apparent magnitudes at peak < 18.5 so in other words keep all transients brighter than 18.5 magnitudes. The justification for this was that the sample will start to become incomplete at dimmer and dimmer magnitudes, so the cut-off point at 18.5 mags was enough so that the sample was appropriately complete and enough in which the volume of data was not sufficiently reduced. This classification completeness and subsequent loss factors will be covered in slightly more detail in **§3.2**. The next selection cut was to keep the peak times of all transients within the bounds of 200 to 1500 days. The peak time represented when the event was brightest, in days since the 3rd of September 2017. The bounds of 200 to 1500 days may seem arbitrary at first however this was sufficient in keeping the whole dataset within the timeframe from which it was taken. The next cuts were in relation to purity and quality cuts, transients that had the purecode 00 were dropped and transients that contained qualcode 111111 were dropped, these qualcodes and purecodes being related to the quality and purity of light-curve and photometric data gathered in the BTS during candidate classification. The justification for this is related to sample bias. Keeping transients that had poor light-curves would lead to bias within the sample and therefore the estimation of the rates could be very unrepresentative of the true supernova rate densities. The final selection cut was made to remove all non-supernova transients from the sample for example the sample contained objects such as nova and tidal disruption events. So, this was the baseline for selecting and carrying forward the sample for analysis. For easier referencing within this document, the final data-frame after the cuts had been applied will be defined as ***df-alpha***.

The information contained in ***df-alpha*** that were relevant to this analysis were:

- Apparent magnitudes at peak
- Absolute magnitudes at peak
- Rise time, how many days to go from half peak to peak
- The amount of dust extinction (in magnitudes as measured in V-band) along the line of sight to the transient, originating from the Milky Way galaxy.
- Classified supernovae type
- Host galaxy absolute magnitudes
- Peak time - When the event was brightest, in days since 03 Sept 2017.

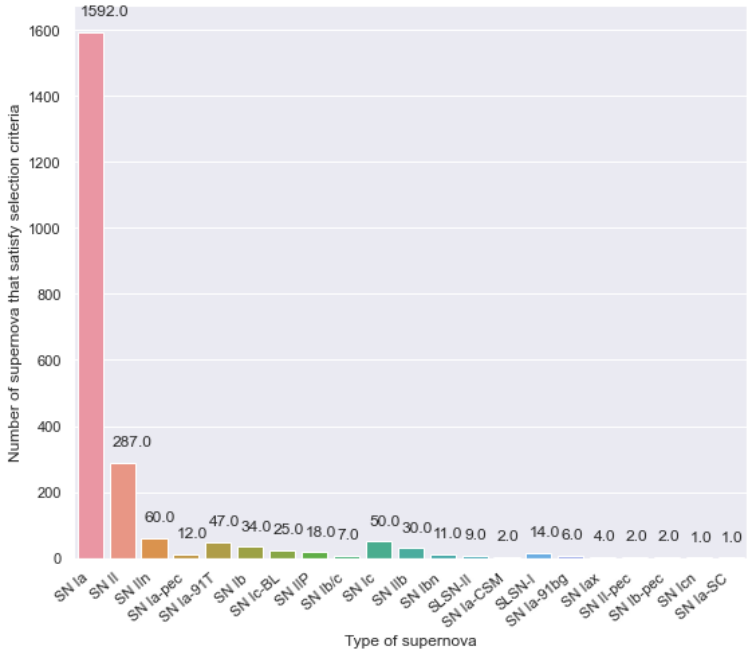

Figure 5 - Graphical representation of the classifications of supernovae in the sample. In total 2214 supernova met the selection criteria given in the flowchart above. This sample is heavily dominated by type Ia with a percentage of $\frac{1664}{2214} \times 100 \approx 75.2\%$ of the total sample and therefore core collapse supernovae make up about 24.8% of the sample. It must be noted that this sample slightly incomplete due to some misses in classification however that is well accounted for within loss factors mentioned in **§3.3**. The data from the BTS sample was taken on the 5th of November 2021.

Figure 5 above shows the sample of supernovae following selection cuts. There were 2214 total supernovae in the sample used with 1664 being type Ia and 550 being Core collapse related. From this we can estimate that the rates obtained from type Ia are going to be more reliable given a larger sample size. The reason for the substantial number of type Ia supernovae is that they are more prevalent at higher luminosities such that they are more easily detected and spectroscopically identifiable hence the considerable number within this sample and that are detected in general.

The next step was to use the data-frame which had been passed through all the selection criteria to evaluate the distribution of Type Ia and core collapse supernovae according to their absolute magnitude at peak. The motivation for investigating this distribution is to determine the magnitude range that will be applied within **§3.2** when calculating the cumulative supernova rates densities.

First ***df-alpha*** was now cut by whether it contained Type Ia or CCSNe. So, now there would be two separate data-frames. Before creating histograms with these two data-frames, the peak absolute magnitudes within the data-frames needed to be converted into float values as initially when loaded they were strings which cannot be used numerically.

The histograms displaying the intrinsic luminosity distributions of type Ia and CCSNe are shown in ***Figure 6*** and ***Figure 7*** respectively below. Normally these figures would find themself in **Chapter IV,** however due to the implication of this distribution on the methodology described in **§3.2,** then it would be better placed here.

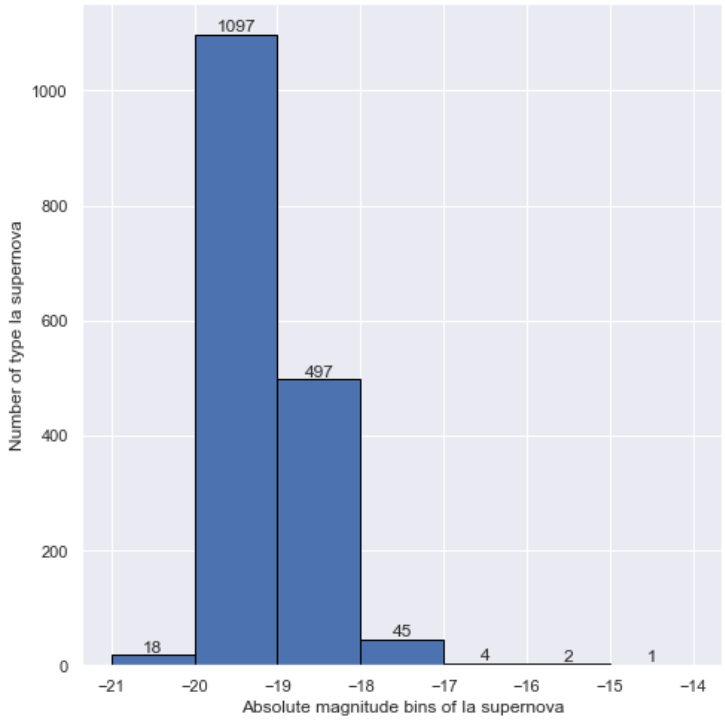

Figure 6 – Histogram for Type Ia which passed selection cuts distributed according to their luminosities. This figure shows the absolute magnitude at peak as a set of one magnitude wide bins going from -14 to -21 with the number of Ia supernova within particular magnitude bins given by the vertical axis. From the figure, type Ia supernova are most frequent within the -19 to -20 bin with 1071 counted within this bin. Type Ia supernova are not common at low luminosities

In ***Figure 6***, the main noticeable point is that there are few supernova at low luminosities from -14 to -17 magnitudes with only a total of three supernova found within this magnitude range. The distribution of type Ia supernovae have a high frequency within the -18 to -19 and -19 to -20 bins.

Taking -17.5 as the midpoint of the peak absolute magnitude range, the distribution of low luminosity (> -17.5) and high luminosity supernova (< -17.5) can be more acutely quantified rather than a mix of a qualitative and quantitative discussion.

In ***Figure 6***, there is a total of 1664 Ia supernova with 1598 of them being counted in the high luminosity half (≈ 96%) of the distribution and 66 (≈ 4%) being counted in the lower luminosity half.

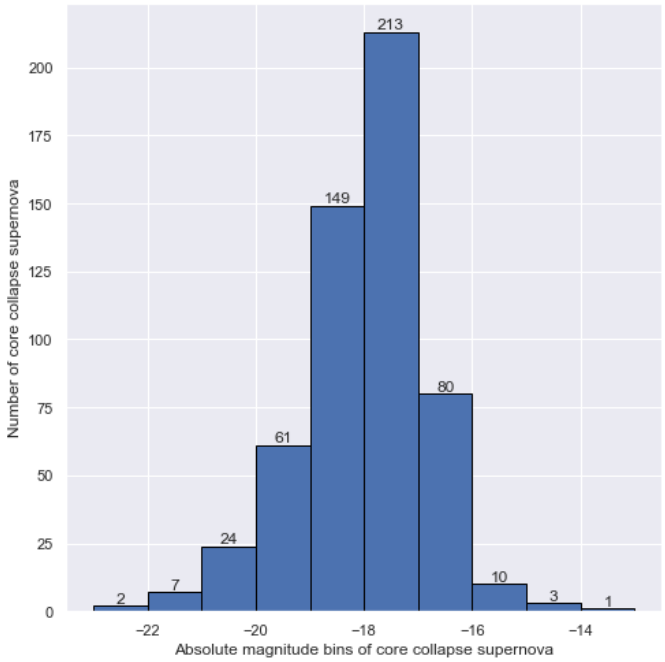

Figure 7 - Histogram of core collapse supernova which passed selection cuts. This figure shows the absolute magnitude at peak as a set of one magnitude wide bins going from -13 to -23 with the number of CCSNe supernova within particular magnitude bins given by the vertical axis. From the figure, CCSNe supernova are most frequent within the -17 to -18 bin with 213 counted within this bin. CCSNe are slightly more common at higher luminosities than at the lower regime.

In ***Figure 7***, within the cut sample, CCSNe are slightly more common at higher luminosities than at lower luminosities with the most occupied bin being from -17 to -18. In comparison to figure 4, there is a greater spread of CCSNe across this peak absolute magnitude range defined from -13 to -23 (low luminosity to high luminosity) than the Ia supernovae. In ***Figure 5***, there are a total of 550 Core Collapse supernova within this distribution. 354 (≈ 64%) of them being counted in the high luminosity half of the distribution and 196 (≈ 36%) being counted in the lower luminosity half.

3.2 – Inverse Volumetric Rate Method

Now that the luminosity distribution of the sample has now been defined, the volumetric rate method could be implemented. This method follows ***Equation [1]*** established in **§2.2**. The motivation for using a rate calculation which depends inversely on the detection volume is the idea that taking a volume out to each supernova ensures that it is included within the rate whereas in an alternative method it may be excluded.

Given that any real SN survey will not cover the whole sky and operates over a limited time duration and must contend with extinction as well as not recovering all detected transients then the loss factors mentioned above were necessary to compensate for these issues.

f_{sky} represents the average sky survey footprint as a fraction of the whole sky. This was estimated by eye to be 0.36 using ***Figure A1*** in the appendix.

$f_{cl,i}$ represents the classification efficiency. To estimate this, the BTS sample explorer was used and only events that satisfied quality, purity cuts and that were brighter than 18.5 magnitudes at peak were viewed. The estimation involved looking through these events since July 2020 and estimating how many of them could have been classified as supernova based on their light-curves in comparison to the total number that were classified as supernovae over this period. There were 1095 supernova classified within the mentioned conditions. After visually inspecting unclassified events under the same conditions, seventeen of these events seemed as if they could have been supernova therefore giving a classification efficiency of $1 - \frac{17}{1095} \approx 0.98$. However, since this estimation was only made over the period from July 2020 which was effectively only half the total time duration of 3.56 years, it was therefore appropriate to take an average between the value given in Perley et al (0.9) as this was calculated from around the first half of the total time duration. The average of these two values is 0.94. Given that it is only a minor correction, it will not affect the rate estimation so much if the classification efficiency is slightly different than estimated.

f_{ext} is the average reduction in effective survey volume due to Galactic extinction. The value of 0.82 from Perley et al was taken as a reasonable estimate for this parameter. Normally it would be calculated by averaging the reduction in volume associated with the extinction toward each separate Zwicky Transient Facility field. There were no means to calculate this parameter in this analysis, so the value was assumed to be reasonable.

Finally, f_{rec} is the average recovery efficiency for a detectable transient within the survey footprint: the probability that it is found and included in the sample. The number of classical nearby Ia supernovae which peaked within the observation window which passed the magnitude cuts of $M_i < -18.5$ and $m < 18.0$ but not the quality cut was estimated to be 413. The number that did pass all conditions and the quality cut was 744 so taking the fraction of $\frac{413}{744+413} = \frac{413}{1157} = 0.64$, this value was taken as the recovery efficiency.

An interesting feature which these loss factors uncover lies within the classification efficiency. Given that the classification given in Perley et al was taken from the start of observation to July 2020 (2.44 years) and the estimation made for this analysis following everything after July 2020, there is a noticeable increase in classification efficiency in the second half, an 8% increase. Of course, these values may be

slightly ideal however it is noted that they have improved their classification routines recently so perhaps this number is to be expected.

Now that the loss factors have been accounted for and estimated, the next step was to begin to define functions which could systematically work through the data-frames and produce supernovae rate curves. An example of one of these functions is a screenshot given as ***Figure A2*** in the appendix.

The main idea in these functions was for it to take data-frames which will have now been cut by supernovae type from ***df-alpha*** and use these to calculate the cumulative rate. The main idea was to have individual rates calculated which were the multiplication of the inverse volume and inverse of the loss factors as seen in ***Equation [1]*** for each supernovae.

To turn these individual rates into a cumulative total rate, the idea was to use an effective limiting magnitude range. This was done using a for loop which followed that for n in the limiting magnitude range, any supernovae with peak apparent magnitudes greater than n would be cut from the provided data-frame. Then the remaining individual rates would be summated and divided by the total survey time of 3.56 years at each magnitude value. Essentially increasing the number of supernovae at brighter apparent magnitudes as the for loop carries forward which summates each individual rate together. Each detection volume calculated was extinction corrected through $D_{max,i}$ where $D_{max,i}$ was calculated from the distance modulus formula (See appendix) which involved making us of a limiting apparent magnitude (18.5) and the peak absolute magnitudes of the supernovae.

The interesting question here relates to what magnitude that each supernova type is taken out to when performing the cumulative rate calculation and this lies with the luminosity distributions, seen in ***Figure 4*** and ***Figure 5***. Let us take the rate calculations for Ia vs CCSNe as an example as these were the main focus of this analysis. Given that there was very few Ia out to a magnitude of -14, i.e., very dim luminosities therefore it was concluded that it would be inappropriate to use the full magnitude length of -14 to -23, for Ia as incompleteness would be an issue, the magnitude range that was thought to be most appropriate was from -16.5 to -20.6 and for CCSNe, the reason of more supernovae at dimmer luminosities being present, the limiting magnitude range for CCSNe rate calculation was taken from -14 to -20.6. Taking the Ia cumulative rates from -14 to -20.6 would have been unrepresentative of the sample and Ia SNe in general. It is important also to note that these magnitude ranges decreased in measures of 0.005 magnitudes, whilst it is a ridiculously small increment, it allows for many data points and cumulative rates to be plotted which is always a bonus and only aids the estimation of the rates at given magnitudes.

Now that these cumulative rates were calculated for Ia vs CCSNe, they were plotted on axes with cumulative rate(y) vs limiting absolute magnitude(x), this will be seen in **§4.2.**

Similar analysis was performed for types; II, IIn, Ib, Ic and Ia-91T, it was taken as fair estimate to assume that all CCSNe subtypes should follow a similar luminosity distribution of -14 to -20.6 and all Ia supernovae would follow the luminosity distribution going -16.5 to -20.6. The next step was to provide upper and lower limits to the rate estimates.

3.3 – Bootstrapping Technique and Upper Confidence Limit

As mentioned in **1.3**, a bootstrapping technique needs to be applied in situations where there is no natural form or theory that can describe the error margins. In the case for these cumulative rates, 95 % confidence intervals were calculated. The 95% confidence intervals were calculated by taking the initial data-frames, so those of which that were derived subsequently from **df-alpha** and then resample them with replacement and calculate the cumulative rate in the exact same way as in **§3.2** however this cumulative rate calculation is conducted four thousand times for each magnitude in the magnitude ranges which are also defined in **§3.2**. All these cumulative rates for each magnitude are appended into an array where a function calculates 95% confidence intervals.

SNe Type	Limiting Absolute Magnitude Range	Total Number of Iterations ($\times 10^6$)	Run Time
Ia	[-16.5, -20.6, -0.005]	3.28	≈ 1 *hour*
CC	[-14, -20.6, -0.005]	5.28	≈ 1.5 *hour*

Table 1 – Table showing the limiting absolute magnitude ranges for both Ia and CC supernovae along with the total number of iterations required for a full 95% confidence interval treatment of every single magnitude data point for each sample. These iterations took about 1, 1.5 hours to complete for each supernova type given the total iterations were in the millions (3,280,000 and 5,280,000 for Ia and CCSNe respectively)

Table 1 provides the computational side of applying the bootstrap technique to the data samples. Whilst the long run times (1-1.5 hours) were a slight concern, the benefits of such a complete analysis of the rates at incremental magnitudes outweighed this issue. ***Figure A3*** in the appendix will provide an example screenshot of the code used to perform a bootstrap. The next step was to apply an upper 95% Poisson confidence limit for zero observed events at a given magnitude. This was a quite simple procedure, the formulism follows:

$$R_{upper} = \frac{1}{T}\sum_{i=1}^{N} \frac{3.69}{\left(\frac{4\pi}{3}D_{max,i}^{3}\right) f_{sky} f_{cl,i} f_{ext} f_{rec}} \quad \textbf{Equation [3]}$$

Equation 3 follows from a table of known values such that the confidence intervals for the expected value, λ of a poisson random variable. For N, observed events the 95% upper confidence limit is equivalent to 3.69. To do this a range of peak absolute magnitude values were selected in an array going from -13 to -20.6 in -0.005 intervals and the same analysis performed in **§3.2** was taken to produce an upper confidence limit line at zero events for each cumulative rate plot produced.

The next section of the methodology involves estimating rates based on host galaxy luminosity of Ia and CC supernovae.

3.4 – Rates as a Function of Host Galaxy Luminosity

The methodology involved in estimating rate densities based on host galaxy properties such as the host luminosity is extremely similar to the methodologies described in both **§3.1** and **§3.2** however the key distinction comes in an additional selection cut. This selection cut involves cutting the data sample by host galaxy absolute magnitude bins. These were bins with widths of one magnitude. For example, this involved taking **df-alpha** and applying the usual selection cuts that were described in **§3.1** but an

additional selection cut in which the derived data-frames for Ia and core collapse SNe were cut again by only keeping supernovae that for example have host galaxy absolute magnitudes between -15 and -16. Since the host galaxy luminosity distributions went from -15 to -23 for both Ia and CCSNe (See ***Figures 10,11 in* §4.1)**, then consequently, one magnitude wide bins through this range were used to cut the sample. So, this would lead to sixteen new data-frames for Ia and core collapse SNe (8 for each) derived from cutting by host galaxy luminosity.

For each of these data frames, the supernovae rate densities and associated 95% confidence intervals could be calculated as stated in **§3.2** and **§3.3**, however following obtaining these rate densities, the next step was to make plots in which the rate densities are plotted as functions of the host galaxy absolute magnitude bins defined prior with each SNeRD being placed at the midpoint of the luminosity bins. These figures can be found in **§4.1** (See ***Figures 8 and 9***). Polynomial curves have been fitted to the figures shown in **§4.1** and a R squared value calculated for each of these fits. The motivation for this is to show the distributions easily for the reader.

3.5 – Converting SFRDs to SNeRDs

As discussed in **§2.2**, the SFRD calculated in literature can be converted into a supernovae rate density by the use of Equation **[2]** and setting the upper and lower mass limits to $45M_{\odot}$ and $8M_{\odot}$ respectively. The reason for these mass limits is that CCSNe are often quoted as having a mass range from eight to either 40 or 50 solar masses, therefore it was best assumed to take the midpoint of this upper mass limit. The methodology here is extremely simplistic and very brief.

The critical point to make first which has been made in **Chapter I** is that only star formation rate densities at significantly low redshift $0 < z > 0.1$ were taken from the literature due to the sensitivity of the ZTF and BTS at low values of redshift. Obviously, this was done to keep the analytical comparisons fair and consistent as one would surely find that comparing a SNeRD derived from a SFRD taken at high redshift would yield very drastic results to that which has been obtained in this study. SFRDs were taken from literature which were usually given in logarithmic form (see column one of ***Table 4***). These were subsequently converted (along with their statistical uncertainties) into SNeRD's by use of ***Equation [2]*** in **§2.3**, where the efficiency of forming CCSNe is calculated to be $6.9 \times 10^{-3}\ M_{\odot}^{-1}$ from upper and lower mass limits of 45 and 8 solar masses, respectively. Subsequently these were compared with the CCSNe rate density obtained in this study and discussed in **§5.4**

Chapter IV: Results

4.1 – SNeRDs and Demographics in Relation to Host Galaxy Luminosity

This sub-section will cover the results obtained via the methodology described in **§3.4** where Supernovae rate densities have been calculated within data samples that have been cut by the luminosities of the host galaxy. It will also cover the demographics or in other words the number of type Ia SNe or CCSNe that are within each of the one wide host galaxy absolute magnitude bins ranging from -15 to -23.

Figure 8 shows a plot of cumulative rate densities for type Ia SNe as a function of host galaxy magnitude, which ranges from -15 to -23. There is a steep increase in the rate with increasing galaxy brightness until a fall after -22 mags. The peak cumulative rate density is $8.04\pm^{0.98}_{1.0} \times 10^3\ Gpc^{-3}\ yr^{-1}$ in the -21 to -22 host galaxy luminosity bin. A fifth-degree polynomial curve was fitted to this data which had a R squared value of 0.996

Figure 9 is a similar plot to ***Figure 8*** in that it shows the cumulative rate densities for CCSNe as a function of host galaxy magnitude, which ranges from -15 to -23. There is an increase from -15 to -17 magnitudes however the rate density falls at galaxies with luminosities between -17 and -18 magnitudes giving this curve a shoulder. After this the rate density increases similarly to ***Figure 8*** with a peak cumulative rate density of $1.91\pm^{1.1}_{0.69} \times 10^4\ Gpc^{-3} yr^{-1}$ in the -21 to -22 host galaxy luminosity bin, however this peak value has very large error intervals which overlap with the rate density value in the prior bin. The rate density falls again after -22 mags. A fourth-degree polynomial curve was fitted to this data which had a R squared value of 0.977

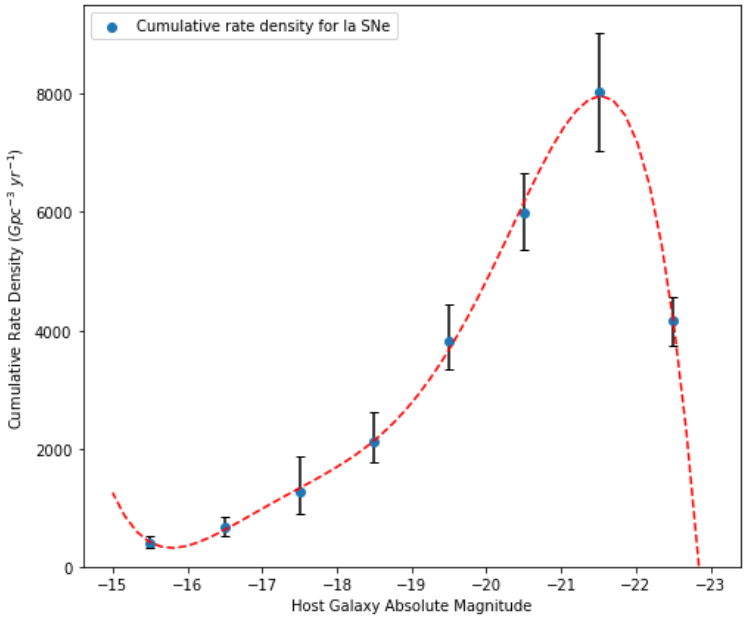

Figure 8 – A plot of cumulative SNe Ia rate densities as a function of host galaxy magnitude with a 5th degree polynomial curve fitted. Each rate density is plotted at the midpoint of each of the one magnitude wide luminosity bins. Ninety-five percent confidence intervals from bootstrapping are given by asymmetric error bars. There is a steady increase in SNe Ia rate as the luminosity of galaxies increases until it drops off after -22 magnitudes.

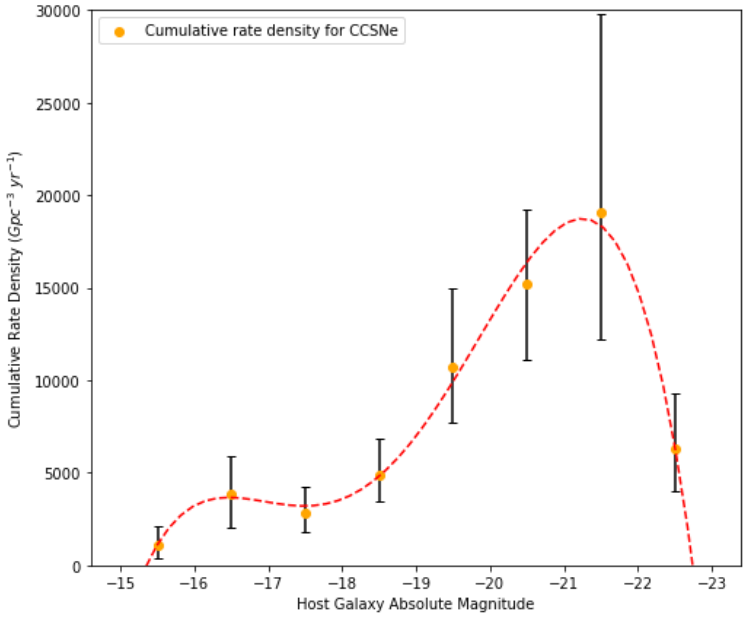

Figure 9 – A plot of cumulative CCSNe rate densities as a function of host galaxy magnitude with a 4th degree polynomial curve fitted. Each rate density is plotted at the midpoint of each of the one magnitude wide luminosity bins. Ninety-five percent confidence intervals from bootstrapping are given by asymmetric error bars. There is a short increase in CCSNe rate as the luminosity of galaxies increases until it drops between -17 and -18 magnitudes but there after there is a similar rise but albeit less steep to Figure 8 as host luminosity increases with a fall after -22 magnitudes

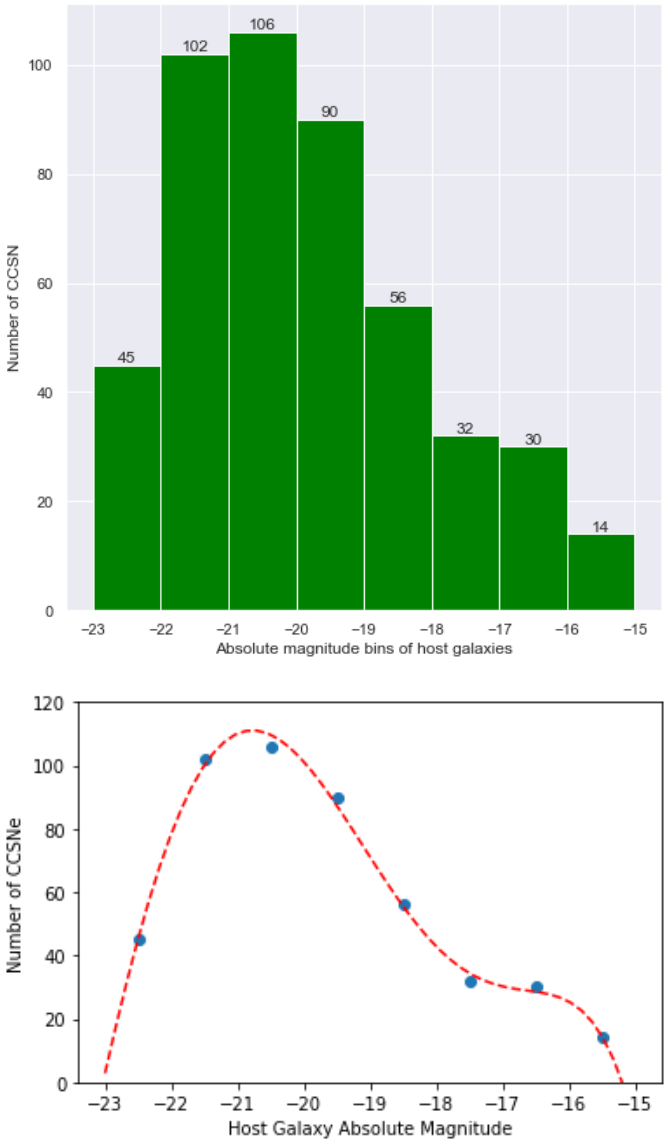

Figure 10 – Top panel displays histogram plot showing the distribution of CCSNe as a function of the absolute magnitude of host galaxy. Each bin is one magnitude wide and this ranges from -15 to -23 magnitudes. The most frequented bin is that between -20 and -21 magnitudes with 106 CCSNe found in galaxies in this luminosity band. The lower panel shows a fifth-degree polynomial fitted to this distribution of CCSNe.

The upper panel of ***Figure 10*** is a histogram which shows the distribution of CCSNe as a function of the intrinsic luminosity of the galaxies they were found in. The most frequented bin is host galaxies with

absolute magnitudes between -20 and -21 and the least frequented bin was host galaxies which had absolute magnitudes between -15 and -16, therefore there are few CCSNe found in dim galaxies. The lower panel of ***Figure 10*** displays a fifth-degree polynomial fit to the distribution of CCSNe. This polynomial fit had an R squared value of 0.987.

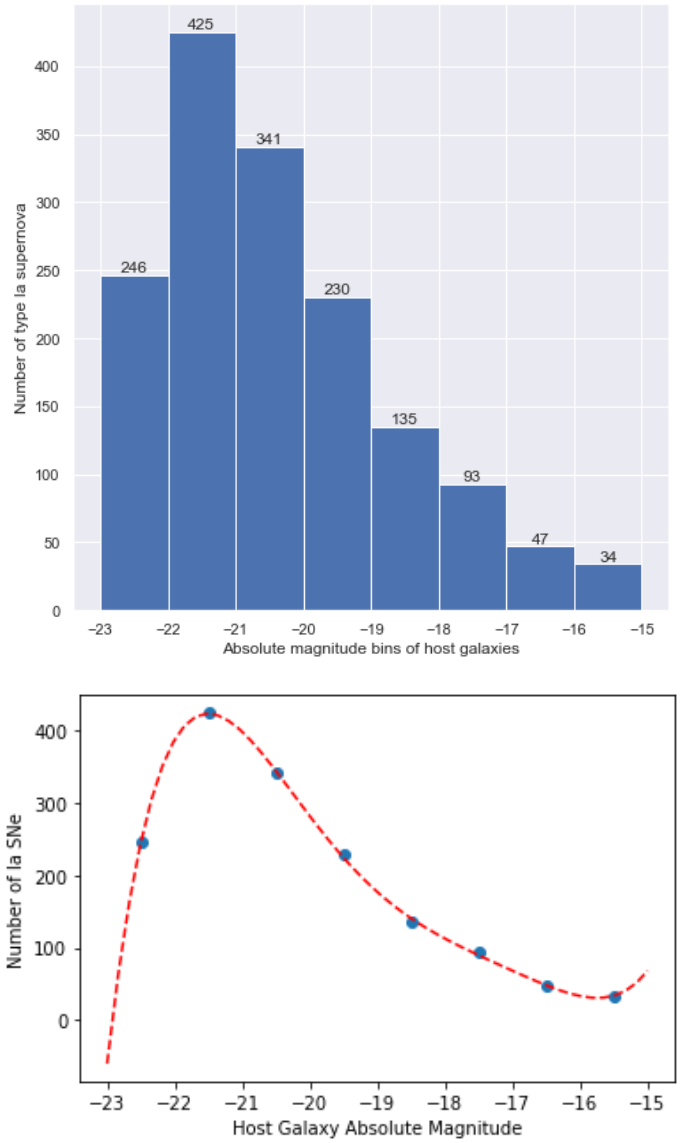

Figure 11 – The top panel displays a histogram plot showing the distribution of Ia SNe as a function of the absolute magnitude of host galaxy. Each bin is one magnitude wide and this ranges from -15 to -23 magnitudes. The most frequented bin is that between -21 and -22 magnitudes with 425 Ia SNe found in galaxies in this luminosity band. The lower panel shows a fifth-degree polynomial fitted to this distribution of Ia SNe.

The upper panel of ***Figure 11*** is a histogram which shows the distribution of Ia SNe as a function of the intrinsic luminosity of the galaxies they were found in. The most frequented bin is host galaxies with absolute magnitudes between -21 and -22 and the least frequented bin was host galaxies which had

absolute magnitudes between -15 and -16, therefore there are few type Ia found in dim galaxies. The lower panel of ***Figure 10*** displays a fifth-degree polynomial fit to the distribution of Ia SNe. This polynomial fit had an R squared value of 0.998. The population of Ia SNe is skewed towards more luminous galaxies.

However, despite there not being many CCSNe or Ia in dimmer galaxies, there are more Ia in dim galaxies than CCSNe. For example, in the host galaxy absolute magnitude bins going from -15 to -16 to -17, there is approximately 1.84 times more Ia in this host galaxy absolute mag range than CCSNe.

In terms of the shape of the distributions, the distribution shown in the lower panel of ***Figure 10*** has a wider peak than that of the polynomial fit of ***Figure 11***, which has a much narrower peak and an incline which when moving from dimmer to brighter host galaxy absolute magnitudes is not as steep as the incline when moving across the same luminosities in the lower panel of ***Figure 10***.

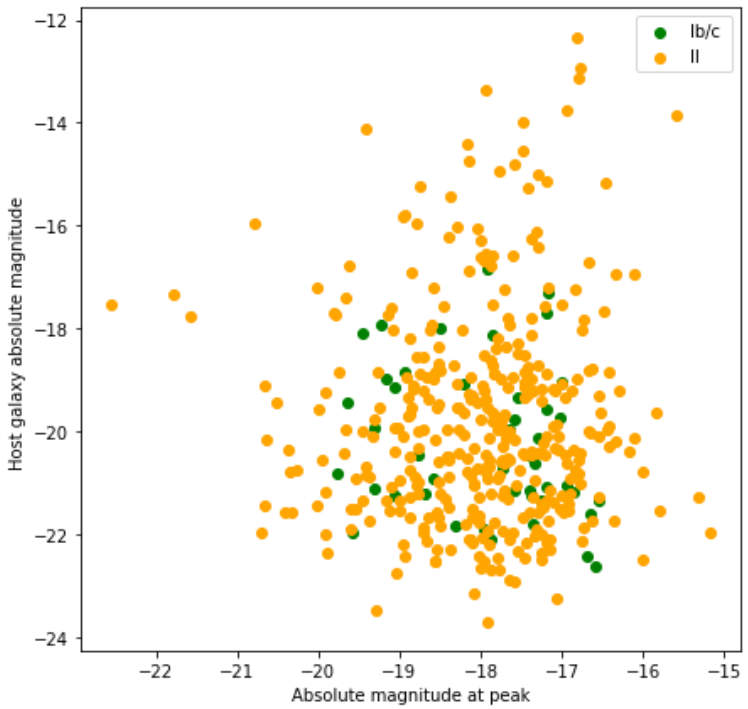

Figure 12 – Host galaxy absolute magnitudes of Ib/c and II SNe as a function of their absolute magnitude at peak. The distribution of these supernovae of both types (core collapse and stripped core collapse) are distributed within the same regions.

Figure 12 shows the distribution of Type II (core collapse) and Ib/c (stripped core collapse) SNe across their intrinsic luminosity properties and the host galaxy luminosity they were found in. The distributions of these two types of SNe is remarkably similar, the only noticeable difference coming in the significantly lower count of Ib/c SNe.

4.2 – Experimental Rate Density Values and SNeRD Plots

This sub-section will consist of the results regarding eleven supernovae rate densities gathered by use of the methodology in **§3.2.** A plot displaying CCSNe and Ia rate densities as functions of limiting absolute magnitude is also given as well as a plot between type II, Ib and Ic of the same form.

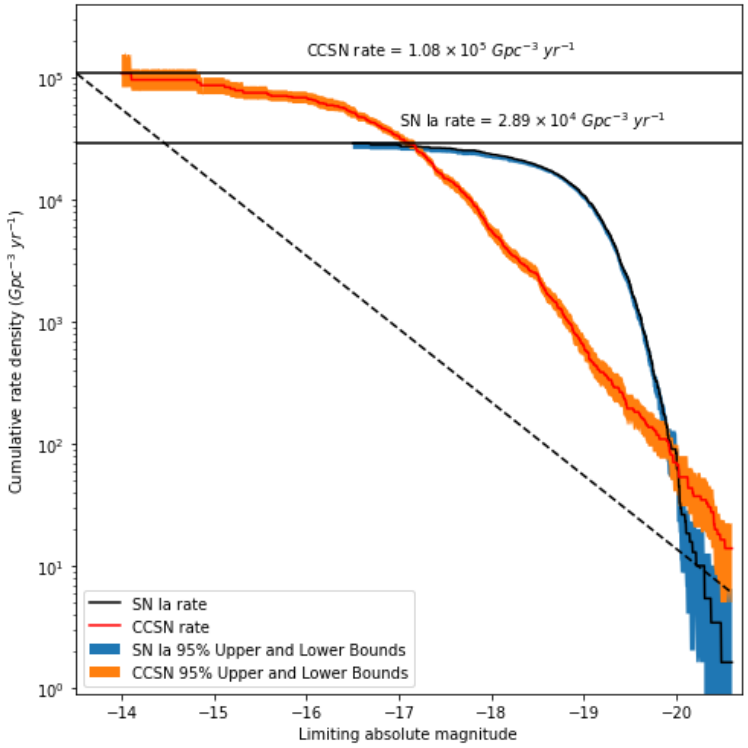

Figure 13 – Rate density measurement curves for Type Ia (including Ia subtypes) and CCSNe. Here the plot shows the volumetric rate of the particular SNe type brighter than a particular absolute magnitude; The orange and blue bands correspond to 95% statistical confidence intervals for CCSNe and Ia SNe, respectively. Horizontal solid lines show the total Ia rate (to −16.5 mag) and CCSNe rate (to −14 mag) estimated from this study. The black dashed diagonal line indicates statistical upper limits (95% confidence) for the case of zero detected events at a given magnitude to account for the ineffectiveness of a bootstrap at dim and bright luminosities (see again **§3.3**)

Figure 13 is a plot showing rate density estimations for both type Ia SNe and CCSNe as a function of limiting absolute magnitude. The plot represents rate densities for SNe brighter than a particular limiting absolute magnitude. The orange and blue bands correspond to 95% confidence intervals for CCSNe and Ia SNe respectively (see **§3.3)**. The figure which displays the CCSNe vs Ia (without subtypes) can be found in the appendix (see ***Figure A4***)

As described in **§3.2,** Ia and CCSNe were taken out to different limiting magnitudes as can be seen in ***Figure 13*** with Ia taken out to -16.5 and CCSNe taken out to a limiting absolute magnitude of -14. The rate estimates are shown by the horizontal lines in this figure. Therefore, the rate density for CCSNe

brighter than -14 magnitudes is $1.08\pm^{0.54}_{0.24} \times 10^5\ Gpc^{-3}yr^{-1}$ and the rate density for Ia SNe (including Ia subtypes) brighter than -16.5 magnitudes is given by $2.89\pm^{0.21}_{0.19} \times 10^4\ Gpc^{-3}yr^{-1}$.

For comparison if the rate density of CCSNe brighter than -16.5 magnitudes is taken ($5.17 \times 10^4\ Gpc^{-3}yr^{-1}$) and compare this to the Ia rate density, the ratio of these quantities is approximately 1.8. Therefore, it is expected that in a cubic gigaparsec every year that twice as many CCSNe occur than Ia SNe.

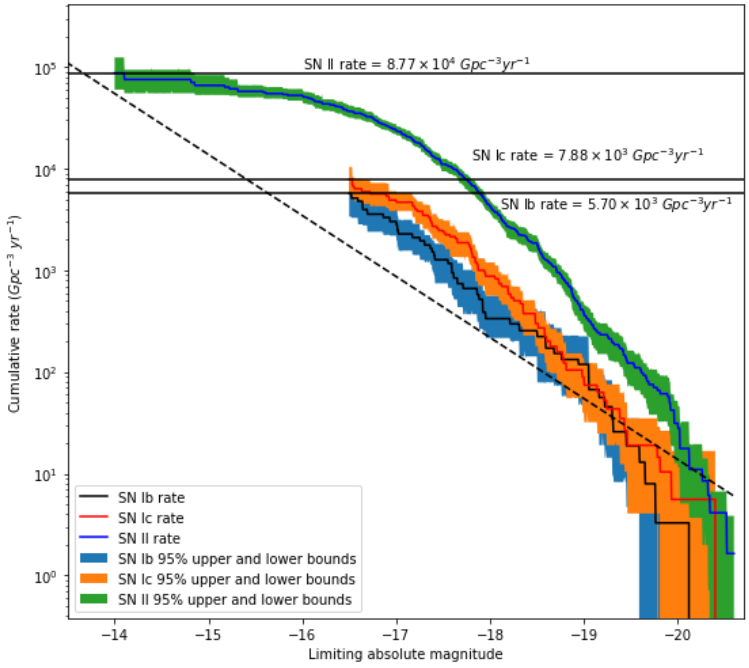

Figure 14 - Rate density measurements for Type II, Ib and Ic SNe (including subtypes for each). Here the plot shows the volumetric rate of the particular SNe type brighter than a particular absolute magnitude; The orange, blue and green bands correspond to 95% statistical confidence intervals Type II (including II subtypes), Ib and Ic SNe, respectively. The black dashed diagonal line indicates statistical upper limits (95% confidence) for the case of zero detected events at a given magnitude to account for the ineffectiveness of a bootstrap at dim and bright luminosities (see again **§3.3**)

Figure 14 is another rate density plot for the SNe types of II, Ib and Ic. The rate density for type II SNe with M <-14 is $8.77\pm^{3.7}_{2.8} \times 10^4\ Gpc^{-3}yr^{-1}$ and the rate densities for type Ib and Ic SNe with M < -16.5 is $5.70\pm^{2.0}_{2.3} \times 10^3\ Gpc^{-3}\ yr^{-1}$ and $7.88\pm^{2.6}_{2.2} \times 10^3\ Gpc^{-3}yr^{-1}$ respectively.

The rates of Ic and Ib supernova are similar with type Ic SNe being estimated to occur ≈ 1.4 times more often every within a cubic Gpc.

As ***Figure 5*** showed type II SNe dominate the cut sample more than any other core collapse supernova accounting for 72% of the CCSNe in this study. Comparably as ***Figure 14*** shows; type II SNe dominate over both Ib and Ic rates even when only type II SNe brighter than -16.5 mags are considered.

Therefore, this study finds that type II supernovae make up a substantial proportion of CCSNe that occur in the universe.

Further SNeRD values can be found in ***Table A1*** in the appendix of this paper.

V. Discussion

5.1 – Discussion and Interpretation of Demographics and SNeRDs

Figure 5 displays the sample demographics following selection cuts described in **§3.1**, the most apparent article for discussion within this figure comes from the proportions of SNe in particular the number of Ia to CCSNe. There are approximately three times as many Ia SNe than CCSNe in the sample of this study. However, this is expected as type Ia typically have far brighter luminosities compared to CCSNe, so they are far easier for the BTS to detect and classify. CCSNe also suffer from far more from dust extinction than Ia SNe at all redshifts (Smartt, 2009)

It is also noticeable from ***Figure 14*** that Type II SNe dominate the CCSNe group followed by types Ic and Ib. An explanation for the dominance of type II SNe comes again from the typical luminosities and light curves of these types. Typically type II SNe are more luminous than Ic and Ib supernova and Ic SNe are more luminous than Ibs which would suggest that type II supernovae are detected and classified more than Ic and Ib SNe, and Ic are classified and detected more than type Ib SNe.

It is also possible that the underlying mechanisms responsible for a type Ib and Ic SNe to occur is not as common as type II supernovae and has sufficient impact on the luminosity. Essentially type Ib and Ic SNe supernovae are said to occur via the core collapse event (see **§1.1**) of a naked helium star. Stellar winds or a close companion (similar to the progenitor system of Ia SNe) strip away the hydrogen envelopes resulting in a mass loss or mass transfer, respectively. It is possible for bright Ib and Ic SNe occur from massive helium stars undergoing rapid rotation however these mechanisms and conditions are found to be extremely rare in nature (Guetta & Della Valle, 2007) which would explain both the number fraction in ***Figure 5*** but also the estimated SNeRD in ***Figure 14***. Massive, stripped helium stars also have the potential to become blackholes leaving very faint or no SNe at all, again this could explain what is seen in regard to Ib and Ic supernova in this study.

In ***Figures 6 and 7*** the luminosity distributions of Ia and CCSNe are vastly different with the CCSNe sample showing a much broader distribution across absolute magnitude bins than the Ia sample.

Figures 8 and 9 show cumulative rate densities of Ia and CCSNe respectively as functions of the host galaxy magnitude band they were calculated from. To clarify that statement more clearly and as reminder, in **§3.4** a further selection cut was made to investigate SNeRDs in relation to host galaxy luminosities, this was performed by cutting a sample by keeping supernovae which were within galaxies of specific absolute magnitude bins such as -18 to -19 for example.

Both plots were fitted with curves using polynomial regression curve fitting methods with the best fits being chosen according to their R squared value which is a measure of how good a fit is to the data given. The curve in ***Figure 8*** had an R squared value of 0.996 after being fitted with a fifth-degree polynomial model and the curve in ***Figure 9*** had an R squared value of 0.977 after being fitted with a fourth-degree polynomial model. These R squared values are high quantifying a good model fit to the data. Given that the SNeRDs are precisely calculated estimations, the polynomial fits can be interpreted as appropriate for this data as sometimes high R squared values do not always signify a good fit. The polynomial fits serve to graphically show a distribution of SNeRD across host galaxy luminosities so the R squared values should not affect this discussion majorly.

In ***Figures 8 and 9***, the host galaxy absolute magnitude band with the greatest SNeRD is between -21 and -22 for both CCSNe and Ia SNe. This would suggest that the progenitors of both these classes are favoured in brighter galaxies, although there are potentially many systematic factors to consider. It is also important to note that in ***Figure 8***, the peak SNeRD value has large confidence 95% confidence interval upper and lower bounds which invites much uncertainty into that value being indeed the peak in reality. This could have been caused by the random error introduced into resampling with replacement during the bootstrapping phase. It is important to note that the values obtained from the distribution of host galaxy properties are preliminary and may not always be reliable.

In ***Figures 10 and 11***, the number of CCSNe and Ia SNe are shown as both a histogram plot and a polynomial curve fitted to the data points (with high R squared values). In these distributions the most frequented bin of CCSNe and Ia supernova is in host galaxies with luminosities between -20 and -21, and -21 to -22 respectively. This is expected as brighter galaxies are going to be easier to photometrically retrieve data from of course and typically CCSNe and Ia SNe are found more commonly in spiral galaxies or spiral arms and the central bulges of galaxies respectively which happen to be more luminous than other galaxies such as ellipticals.

In ***Figure 10***, there is a broader peak shown in the distribution. In particular looking at the histogram plot, there are similar numbers of CCSNe between absolute magnitude bins going from -19 to -22.

Overall, this would suggest they can be found typically in more luminous galaxies. In fact, in general the distribution is broad in comparison with ***Figure 11***, this comes from the fact that in general CCSNe are a very diverse group in terms of progenitor properties.

Very low-luminosity galaxies contribute negligibly to the SNe Ia population (5.2%) in comparison to being a larger fraction of the CCSNe population (9.3%). It is also noticeable that the SNe Ia population favours higher luminosities with a narrow peak at galaxies with absolute magnitudes between -21 and -22. On the opposite side very high-luminosity galaxies (absolute magnitude from -21 to -23) contribute approximately 12% more Ia SNe (65% of total sample size) than CCSNe (53% of total sample size)

The number of SNe for both populations fell steeply off at the host galaxy absolute magnitude band from -22 to -23. One feasible explanation for this that galaxies that get to these high luminosities are rare or another explanation is that they outshine any SNe events that occur within making them harder to detect within galaxies this bright and on the opposite end less luminous galaxies are going to be more difficult to detect therefore the number count of SNe within them will be lower.

It must be noted that the sample size of the populations used in estimation and plotting of ***Figures 8-11*** were smaller than the sample sizes shown in ***Figure 5*** as further selection cuts were made to constrain SNe into particular host galaxy absolute magnitude bins and some of the supernova with these populations had missing host galaxy photometry data therefore had to be removed from the sample. It is possible that these SNe if they had photometry data would certainly affect the distribution in some manner however it is unknown as to how much it would have affected the distributions of SNe across host galaxy luminosities. Although it is definitely a source of uncertainty.

Figure 12 shows that there are statistically insignificant differences in the distributions of Type II and Ib/c SNe according to their luminosities and host galaxy luminosities. This supports a claim in Perley et al (2020) that line-driven wind stripping does not play a significant role in the loss of the hydrogen envelope from their progenitors given their similar host galaxy properties. Although it must be noted that the number counts of Ib and Ic SNe are much smaller than type II SNe.

5.2 – Comparing Ia Rate Estimates with Values in Literature

SNe Ia Rate Density $10^4 yr^{-1} Gpc^{-3}$	In Agreement?	Redshift	Reference
$2.89 \pm^{0.21}_{0.19}$ [2]	N/A	0.06	This Work
2.40 ± 0.7	Yes	0.01	(Cappellaro, et al., 1999)
2.65 ± 0.34	Yes	$z < 0.014$	(Li, et al., 2011)
$2.59 \pm^{0.52}_{0.44}$	Yes	0.1	(Dilday, et al., 2010)
2.35 ± 0.24	No	≈ Similar to this work*	(Perley, et al., 2020)
2.43±0.29	Yes	$z \leq 0.09$	(Frohmaier, et al., 2019)

Table 2 – Table displaying the SNe Ia rate density estimated in this study along with estimations found in literature. Only estimations made at low redshift in literature were considered for comparison for consistency reasons. Four-fifths agree with the estimation made in this work with the work done by Perley et al in 2020 being the only discrepancy. *Used ZTF and BTS data.

Whilst the Ia rates obtained in this paper are doomed to be affected by systematic errors which aren't easy to quantify, it is very encouraging that the estimation for the SNe Ia rate density shown above in ***Table 2*** agrees with the works done by (Cappellaro, et al., 1999) , (Li, et al., 2011) , (Dilday, et al., 2010) and (Frohmaier, et al., 2019) and it is important to note that the rate density for Ia SNe using only classical Ia supernova is in agreement with these studies.

However, the estimation obtained in this work cannot verify the low rate estimated by (Perley, et al., 2020). Even when comparing with the SNeRD estimate that used classical Ia SNe only (without Ia subtypes), the rate estimations still are not in agreement with the value obtained by Perley et al in 2020

[2] SNe Ia rate density estimated using a sample containing classical SNe Ia and rarer subtypes of type Ia such as Ia-91T

(see first row of ***Table A1*** in appendix). Given that both studies use the ZTF and BTS for data, it may appear strange that there is a discrepancy. However, it may be possible to explain this with the classification efficiency calculated in **§3.2**. Although the values may in principle be slightly ideal, the increase in classification efficiency from 0.90 (Perley, et al., 2020) to 0.98 suggest an overall improvement in the classification process and it has been noted in conversation that the ZTF and BTS have done a better job of classifying transients more recently and given that the study performed by Perley et al had a small blip in the cataloguing of transients in march 2020 due to the pandemic and bad weather, this resulted in the loss of Ia SNe (see ***Figure A5*** in the appendix[3]) and this could have adversely diminished their estimated rate for Ia SNe.

Given the high number of Ia SNe that passed selection cuts and were able to be used in the SNeRD estimate, the upper and lower ninety-five confidence intervals are narrow bands (see SNe Ia curve in ***Figure 13***). The confidence levels in this study are the narrowest ($\pm^{0.21}_{0.19} \times 10^4$) compared to the referenced studies shown in ***Table 2***. This would suggest that there is high accuracy associated with this estimation which was calculated using 1664 Ia SNe obtained from measurements in small comoving volumes (low redshift).

5.3 - Comparing CCSNe Rate Estimates with Values in Literature

Table 3 on the next page shows the CCSNe rate densities from this work compared with CCSNe rate density values found in the literature at low redshift. Out of the five quoted literature values, only three agree with the result estimated in this study with the value quoted from Taylor in 2014 coming closest despite a smaller sample size of CCSNe.

The consistency with the value in Perley et al is encouraging as they followed a similar methodology to obtain their SNe rates, thus not only establishing a consistent CCSNe rate but also verifying the methodology of making specific selection cuts and then using an inverse volumetric rate equation for estimates. This methodology is supported at low redshift due to this consistency.

The span of upper and lower confidence intervals seen in Figure 13 was fairly large with respect to previous studies that were not using BTS data. However, this may be due to the low CCSNe count paired with the bootstrapping technique (***§3.3)*** resampling with replacement and then performing the inverse volumetric rate density method (***§3.2)*** iteratively over tiny incremental absolute magnitudes.

[3] A plot regarding the cumulative number of Ia SNe passing cuts recorded in the survey as a function of time

CCSNe Rate Density $10^5\ yr^{-1}Gpc^{-3}$	In Agreement?	Redshift	Reference	Sample Size [4]
$1.08\pm^{0.54}_{0.24}$	N/A	0.06	This Work	550
$1.01\pm^{0.50}_{0.35}$	Yes	≈ Similar to this work*	(Perley, et al., 2020)	313
1.06 ± 0.19	Yes	$0.03 < z < 0.09$	(Taylor, et al., 2014)	89
$0.91\pm^{0.16}_{0.13}$	Yes	0.028	(Frohmaier, et al., 2020)	86
0.58 ± 0.19	No	0.01	(Cappellaro, et al., 1999)	~ [5]

Table 3 - Table displaying the CCSNe rate density estimated in this study along with estimations found in literature. Only estimations made at low redshift in literature were considered for comparison for consistency reasons. Three-fourths agree with the estimation made in this work with the work done by being the discrepancies. *Used ZTF and BTS data. The known sample sizes of CCSNe used to estimate the rate density.

The value from (Cappellaro, et al., 1999) disagrees with the estimation made in this study by a factor by approximately 1.9. Explanations for this may come from that this was an extremely local CCSNe rate estimated almost 23 years ago, and in the 23 years, observation methods to detect and classify SNe spectroscopically have vastly improved. Therefore, a significantly lower CCSNe rate claim from Cappellaro 1999 cannot be confirmed. This notion tends to agree with what is seen in ***Table 3***; CCSNe rate density estimations tend to agree with each other in the most recent decade with overlapping confidence intervals.

The estimate calculated in this study has the largest CCSNe sample size (550) and that is a testament to the effectiveness of the BTS at detecting and classifying supernovae. In particular the CCSNe rate is difficult to calculate in comparison to the Ia rate, as seen the sample size of CCSNe is significantly

[4] Sample size after passing all cuts
[5] Unknown sample size of CCSNe

smaller than that of Ia (Figure 5) and the luminosity distribution of CCSNe is broader (Figure 6) with a large fraction of the populous coming from dim events which are only detectable in small local volumes.

5.4 – Discussion and Comparison between SFRDs and the CCSNe Rate Density in This Study

Shown below is Table 4 which is a tabulation of Star formation rate densities over the last decade. These SFRDs were converted to SNeRDs in §3.5. Subsequently, it is found from looking at this table that six of the ten values are consistent with the value estimated in this study when they are converted into SNeRDs. The value which is closest is given by Gunawardhana et al (2013) using the Sloan Digital Sky Survey, which is approximately 99% of the estimate of this study's value for CCSNe.

However, the four that show significant disagreement are smaller by approximately 2 times than what is estimated in this work (when rounded up or down), this would correspond to the findings of Botticella et al in 2012 who concluded that the star formation rates derived from Hα are a factor of two smaller than the CCSNe rate (Taylor, et al., 2014).

Star Formation Rate Densities from Literature $\log \rho_{SFR}$ $M_{\odot} yr^{-1} Mpc^{-3}$	Derived Supernovae rate densities via Eq [2] $10^5 yr^{-1} Gpc^{-3}$	≈ Ratio between the CCSNe Rate density in this work and that derived from the SFRDs in literature (2SF)	Redshift Range	Agree?	Reference
-2.10 ± 0.11	$0.548 \pm^{0.12}_{0.15}$	2.0	0.001 ≤ z ≤ 0.017	No	Vilella-Rojo et al (2020)
-2.18 ± 0.17	$0.455 \pm^{0.21}_{0.14}$	2.4	0.01 ≤ z ≤ 0.10	No	Westra et al (2010)
-1.64 ± 0.06	$1.58 \pm^{0.23}_{0.20}$	0.68	0 ≤ z ≤ 0.10	Yes	Gunawardhana et al (2013) -GAMA
-1.81 ± 0.06	$1.07 \pm^{0.15}_{0.14}$	1.0	0 ≤ z ≤ 0.10	Yes	Gunawardhana et al (2013) - SDSS
-1.98 ± 0.03	$0.725 \pm^{0.049}_{0.051}$	1.5	0.005 ≤ z ≤ 0.03	No	Gonzales-Delgado et al (2016)
-1.75 ± 0.06	$1.23 \pm^{0.18}_{0.16}$	0.88	0.005 ≤ z ≤ 0.025	Yes	Van Sistine et al (2016)
$-1.76 \pm^{0.13}_{0.05}$	$1.20 \pm^{0.42}_{0.13}$	0.90	0.001 ≤ z ≤ 0.032	Yes	Audcent-Ross et al (2018)
-1.75 ± 0.07	$1.23 \pm^{0.21}_{0.19}$	0.88	0.02 ≤ z ≤ 0.08	Yes	Driver et al (2018)
-2.09 ± 0.29	$0.561 \pm^{0.53}_{0.27}$	1.9	0.03 ≤ z ≤ 0.17	No	Sanchez et al (2019)
-1.79 ± 0.29	$1.12 \pm^{1.1}_{0.55}$	0.96	0.03 ≤ z ≤ 0.17	Yes	Sanchez et al (2019)

Table 4 – Table displaying estimated SFRDs from literature of the nearest decade given in logarithmic form and their subsequent conversions to SNeRDs. All but three show agreement or consistency with the CCSNe rate density in this study. The quoted redshift that these studies worked within is given.[6] *(Vilella-Rojo, et al., 2020)*

The discrepancy between the value given by Vilella-Rojo et al (2020) in Table 4 and this work could be explained by the very small comoving volume (narrow redshift range) that this SFRD was obtained at in which extreme Hα emitters. The cosmic star formation history plot shown in Madau and Dickinson (2014) is supported by this discrepancy given the increase in star formation with redshift until about z = 2. The average redshift in this study is six times higher (see ***Table 3***) than that in Vilella-Rojo et al (2020)

[6] The rest of SFRDs from previous decades can be found in the appendix - ***Table A2***

which would therefore mean it could be argued that higher CCSNe are expected at slightly larger redshift. They argue that the perceived discrepancy between their SFRD estimation and that of a larger value such as the one estimated by Audcent-Ross in 2018 is due to a relation between star formation rate and HI mass being less steep than predicted.

However, the value for CCSNe rate density obtained in this work is consistent at low redshift with values that deny the SNe rate problem (Horiuchi, et al., 2011) and resolve this issue through use of untargeted galactic surveys and including the faint end of a luminosity function without requiring a significant population of obscured SNe. (Mattila et al.2012) and Jencson et al (2019) suggest obscured SNe could exist.

The CCSNe value in this work is consistent with predictions based on low redshift star formation rate density (Madau & Dickinson, 2014). Again, the CCSNe value obtained in Perley et al (2020) was also consistent with the predictions of Madau and Dickinson (2014) thus again verifying the shared inverse volumetric method in obtaining a CCSNe rate density. Despite the consistency across many results, as stated in Taylor et al (2014) there is a large misunderstanding of the stellar evolution in some regard to CCSNe. There could also be many dim CCSNe that evade detection and this in itself is a function of redshift which of course affect and describe the discrepancies. In fact, Equation 2 that was used in this study to convert the quoted SFRDs in literature (Column 1, Table 4) to SNeRDs has some features that could vary. For example, the time and redshift dependent density function could in fact be more complicated. However as stated in (Horiuchi, et al., 2011), the stellar mass range probed by the SFRD is comparable to the mass range giving rise to CCSNe. Variations in the IMF should have only a small effect on the predicted and converted SNeRD.

VI. Summary

In this study, new rate densities of CCSNe and Ia SNe have been established along with the demographics and distributions of these SNe across their luminosities and host galaxy luminosities. This was conducted by taking an unbiased and spectroscopically complete data sample from the BTS sample explorer and applying various justified selection cuts which resulted in having the largest sample sizes of SNe to date to carry these investigations. Then an inverse volumetric rate equation implemented into python which cut and summated SNe by incremental absolute magnitudes to produce rate curves with 95% confidence intervals courtesy of resampling with replacement using a bootstrapping technique was applied. The overall main aim of obtaining SNeRDs for CCSNe and Ia SNe was achieved successfully given the consistency of these new estimations with values from surrounding work in the literature which used

different methodologies. Luminosity and host galaxy luminosity distributions were also investigated for these SNe and further constrained the properties of SNe progenitors and their star forming regimes and mechanisms with particular focus on II and Ib/c SNe. For other studies that wish to follow this methodology and are subject to stricter time constraints, it is recommended that the size of the absolute magnitude increments is increased, this should not adversely affect the rate estimations or confidence intervals given the nature of bootstrapping. A very efficient machine learning technique could be implemented to classify transients more effectively thus maintaining a high classification efficiency of SNe.

The significant advantages of the methodology carried out within this study is that it can be applied for any SNe type across any limiting magnitude range. Even if the SNe types do not have significant counts but do however pass selection cuts, the implementation of an upper 95% confidence interval at zero observed events (Dashed diagonal line seen in ***Figures 13 and 14***).

There is also a significant advantage with using data taken from the BTS sample explorer as it is transient data that contains significant data such as rise and fade times, host galaxy properties and photometric data such as magnitudes at peak. Even when there is missing photometric data or classification data, the advantage of having a data sample across 3.56 years is that enough transients are included that the transients with missing data values can be cut out leaving a sizeable number of SNe remaining to work with. For example, the initial raw data sample taken on the 5th November had 8570 transients. Following selection cuts, this sample was taken down to 2214 SNe. Whilst this is a significant loss of SNe, it left enough classified SNe to provide estimates of consistent rate densities with literature.

There are also some disadvantages associated with the methodology in this study. Firstly, whilst SNe were corrected for galactic extinction (A_V) they were not corrected for host-galaxy extinction. In future this could be something to consider. Secondly, during the bootstrapping phase (***Table 1***), the nature of cutting the samples by incremental absolute magnitudes (-0.005) meant that to obtain complete upper and lower 95% confidence intervals for one SNe rate curve could take at least longer than hour.

As the ZTF and BTS continues through phase II, it is expected to catalogue many more SNe, thus future studies will have a larger sample size to carry out demographics and rate density estimations. This will hopefully provide more representative estimates and demographics especially for rarer subtypes which for now have very low number counts (see ***Figure 5***). Future studies will also benefit from new spectrograph facilities and additional survey collaboration, which will provide a larger and deeper observation of the sky. Given that the initial raw sample size in this study was reduced by about 74%

following selection cuts, this loss of transient data when in the selection phase will hopefully decrease given new spectrograph facilities and additional sky surveys.

The BTS will still remain important to SNe studies given that there will still be a reliance on photometric classification for fainter populations of SNe and this will only aid in growing the reliability of photometric tools. One hopes that the techniques such as bootstrapping, and the inverse volumetric equation can be refined in the future as computational powers increase, and also that this study can be used as a reference and comparison point for SNeRD estimations within the literature for future studies carried out at low redshift.

VII. Appendix

Link to BTS Sample explorer - https://sites.astro.caltech.edu/ztf/bts/explorer.php

$D_{i,max} = 10^{0.2(m_{lim}-M+5-A_V)}$ – This is the limiting distance term seen in ***Equation [1]***

$\xi(m)\Delta m = \xi_0 \left(\frac{m}{M_\odot}\right)^{-2.35} \left(\frac{\Delta m}{M_\odot}\right)$ - IMF (Salpeter, 1955) with ξ_0 representing a local stellar density

$N = \int_{m_L}^{m_u} \xi(m)dm$ - Total number of stars formed with masses between m_L *and* m_u

$M_* = \int_{m_L}^{m_u} M\ \xi(m)dm$ - Total mass in stars born with mass m_L < m < m_u

$\dot{\rho}_* = \dot{\rho}_0 \left[(1+z)^{a\eta} + \left(\frac{1+z}{B}\right)^{b\eta} + \left(\frac{1+z}{C}\right)^{c\eta}\right]^{\frac{1}{\eta}}$ - time dependent density function seen in ***Equation [2]*** relating to the SFR (Horiuchi, et al., 2011) (see their paper for specific parametrisation)

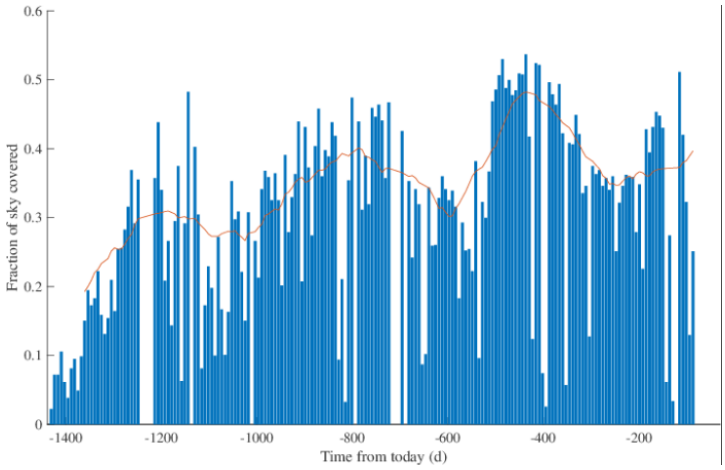

Figure A1 – Sky coverage plot as a function of time since Friday 25th February 2022. This was offset to match survey times in order to estimate the loss factor $f_{sky} = 0.36$. This is only a 10% estimate so making an estimation by eye was sufficient in this case. Provided by Christoffer Fremling.

```
def Rind_multi_Plot(A,B,mlim):
    ######################################## CONSTANTS/APPLICATIONS


    A["peakabs"] = pd.to_numeric(A["peakabs"], downcast="float")
    B["peakabs"] = pd.to_numeric(B["peakabs"], downcast="float")
    mlim = 18.5 #Limiting apparent magnitude
    f = 0.64*0.82*0.94*0.36 # Correction factor values
    Mag1 = np.arange(-16.5,-20.6,-0.005) #Absolute magnitude range for Ia Supernovae
    Mag2 = np.arange(-16.5,-20.6,-0.005) # Absolute magnitude range for CC Supernovae
    ######################################## 1ST DATAFRAME
    muA = mlim - A.peakabs # m-M in the distance modulus formula
    mu2A = 0.2*(muA+5-A.A_V)  # Part II of the distance modulus formula
    dA = pow(10,mu2A) #Distance calculation
    dGpcA = dA*(1E-9) #Conversion from Parsecs to GigaParsecs
    VolA = (4/3)*np.pi*pow(dGpcA,3) # Limiting Volume
    IVA = 1/VolA # Inverse of limiting Volume
    RindA = IVA*(1/f) #Rate for an individual supernova in a sample
    A["RindA"] = RindA #Adding these individual Rates to the Dataframe
    CumSumA = [] #Cumulative Rates
    for n in Mag1:
        yA = A.drop(A[A.peakabs>n].index) #Cutting supernovae from the dataframe by absolute magnitude
        bA = np.sum(yA.RindA)/3.56 #Rate Formula, T = 3.56 yr
        CumSumA.append(bA)       #Cumulative Rates appended
    ########################################


    muB = mlim - B.peakabs
    mu2B = 0.2*(muB+5-B.A_V)
    dB = pow(10,mu2B)
    dGpcB = dB*(1E-9)
    VolB = (4/3)*np.pi*pow(dGpcB,3)
    IVB = 1/VolB
    RindB = IVB*(1/f)
    B["RindB"] = RindB
    CumSumB = []
    for n in Mag2:
        yB = B.drop(B[B.peakabs>n].index)
        bB = np.sum(yB.RindB)/3.56
        CumSumB.append(bB)
```

Figure A2 – Example Screenshot of a function used to calculate SNeRDs for Ia and CCSNe

```
def bootstrap_Ia(n,mlim):
    collective_cumulative_rates = []
    for i in range(0,4000):
        resampled_data = resample(DfIa,n_samples = len(DfIa) ,replace = True, stratify = None
        , random_state = random.randint(1,100))
        resampled_data["peakabs"] = pd.to_numeric(resampled_data["peakabs"], downcast="float")
        f = 0.64*0.82*0.94*0.36
        muA = mlim - resampled_data.peakabs #Essentially mu in the distance modulus formula (m-M)
        mu2A = 0.2*(muA+5-resampled_data.A_V)
        dA= pow(10,mu2A) #Distance modulus
        dGpcA = dA*(1E-9) #Conversion Parsec to GigaParsec
        VolA = (4/3)*np.pi*pow(dGpcA,3) #Volume
        IVA = 1/VolA # Invese of Volume
        RindA = IVA*(1/f) #Individual Rate
        resampled_data["RindA"] = RindA #Adding these individual Rates to Dataframe
        sliced_data = resampled_data.drop(resampled_data[resampled_data.peakabs>n].index)
        #Dataset now left with data cut off  by a particular magnitude level
        cumulative_rate = np.sum(sliced_data.RindA)/3.56 # Rate formula
        collective_cumulative_rates.append(cumulative_rate) #All 4000 cumulative rates calculated from bootstrap
    conf_int = np.percentile(collective_cumulative_rates,[2.5,97.5]) # 95% confidence intervals
    print(conf_int)

for n in np.arange(-16.5,-20.6,-0.005):
    bootstrap_Ia(n,18.5)
```

Figure A3 – An example screenshot of code used to perform a bootstrap in order to obtain 95% confidence intervals for the SNeRD. In this particular case, the bootstrap here is obtaining 95% confidence intervals for the SNe Ia rate density.

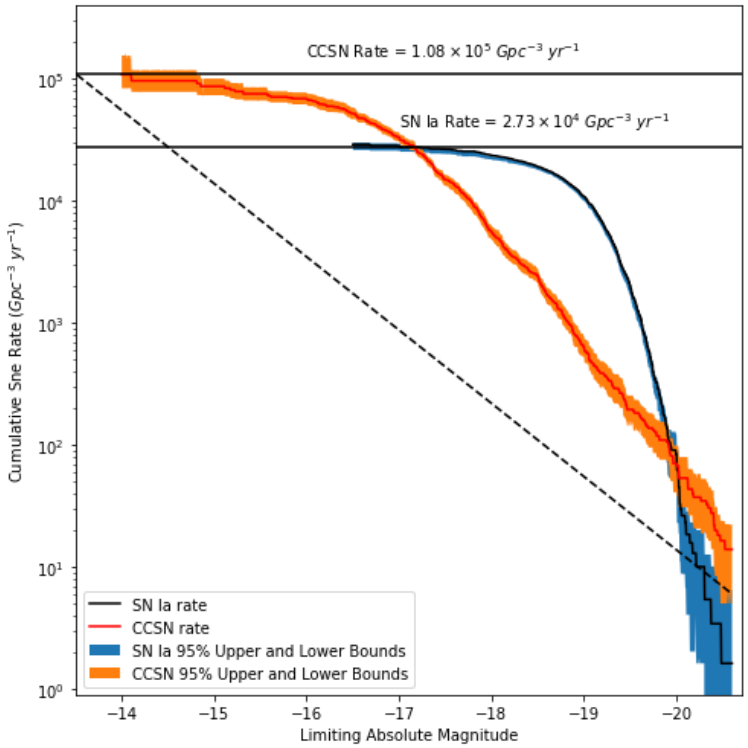

Figure A4 - Rate density measurement curves for Type Ia (excluding Ia subtypes) and CCSNe. Here the plot shows the volumetric rate of the particular SNe type brighter than a particular absolute magnitude; The orange and blue bands correspond to 95% statistical confidence intervals for CCSNe and Ia SNe, respectively. Horizontal solid lines show the total Ia rate (to −16.5 mag) and CCSNe rate (to −14 mag) estimated from this study. The black dashed diagonal line indicates statistical upper limits (95% confidence) for the case of zero detected events at a given magnitude to account for the ineffectiveness of a bootstrap at dim and bright luminosities (see again **§3.3**)

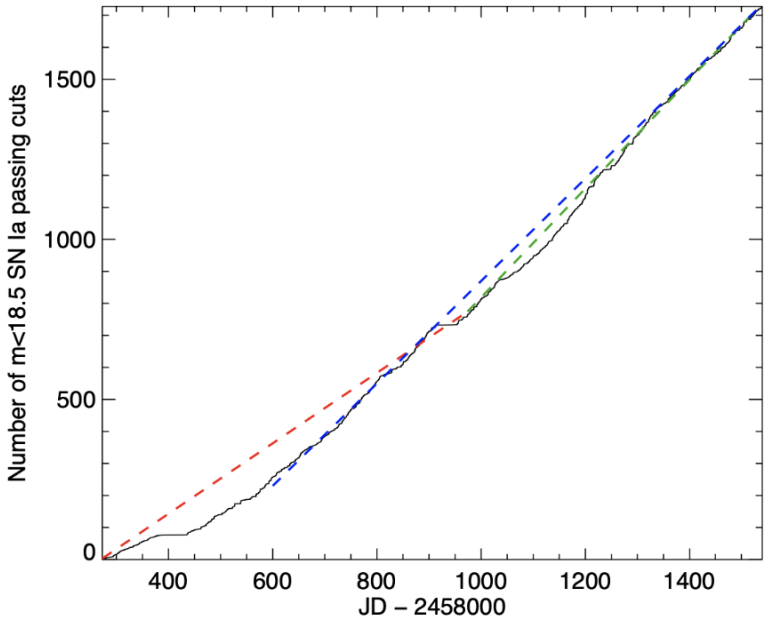

Figure A5 – Plot showing cumulative the cumulative number of Ia SNe (at <18.5 and passing both cuts) recorded in the BTS as a function of time. ZTF was only searching for transients over about half the sky instead of the whole sky during that first year provided by Dan Perley.

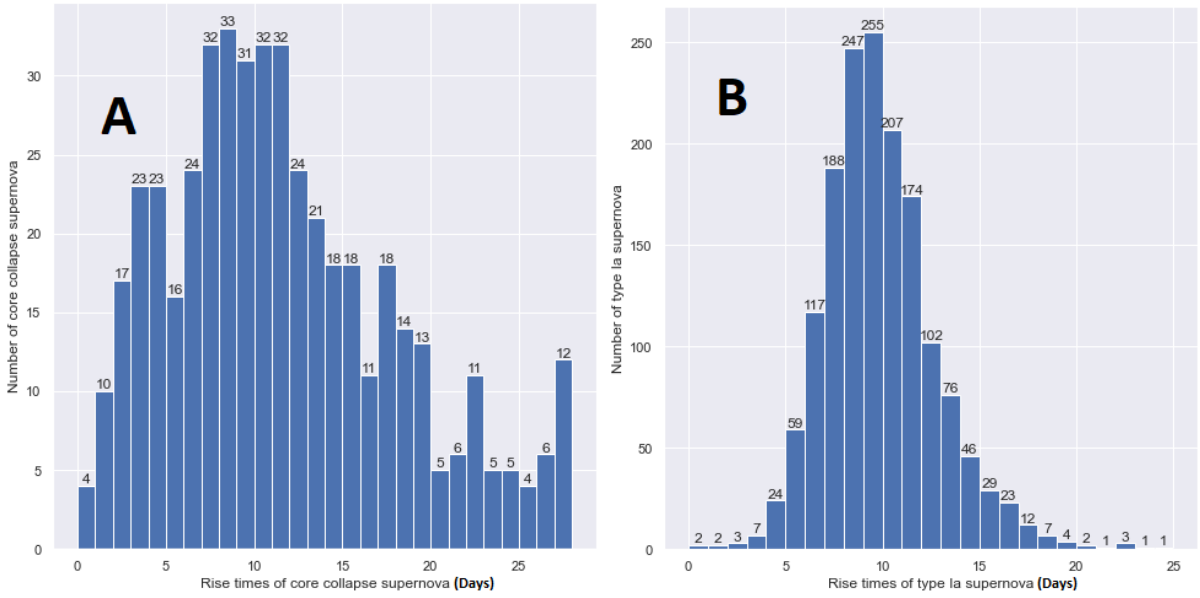

Figure A6 – Two histogram plots showing on the left and right the respective distributions of CCSNe and Ia SNe samples (following selection cuts) with respect to their time taken to go from half-peak to peak in days. A) A broad distribution of CCSNe counts with respect to their rise times. The peak of this distribution is very broad and can be found between rise time bins from 7-13 days. B) A narrower distribution of Ia SNe counts with respect to their rise times. The peak of the distribution is very narrow and found at the 9-10 days bin with a tail on the right side of the distribution favouring longer rise times.

SNe type	Sub sample Size after selection cuts §3.2	Estimated rate density ($Gpc^{-3}\ yr^{-1}$) for SNe brighter than M with given 95% Poisson confidence limits	Minimum absolute magnitude, M
Type Ia	1592	$2.73\pm^{0.26}_{0.13} \times 10^4$	-16.5
CCSNe	550	$1.08\pm^{0.54}_{0.24} \times 10^5$	-14
Type Ia (Including Ia subtypes)	1664	$2.89\pm^{0.21}_{0.19} \times 10^4$	-16.5
Type II (Including II subtypes)	397	$8.77\pm^{3.7}_{2.8} \times 10^4$	-14
Type Ib (Including Ib subtypes *)	47	$5.70\pm^{2.0}_{2.3} \times 10^3$	-16.5
Type Ic (Including Ic subtypes *)	76	$7.88\pm^{2.6}_{2.2} \times 10^3$	-16.5
Type IIn	60	$4.05\pm^{2.4}_{1.7} \times 10^3$	-14
Type Ia-91T	47	$5.12\pm^{1.2}_{1.1} \times 10^2$	-16.5
Type IIb	30	$4.50\pm^{1.5}_{1.3} \times 10^3$	-14
Type IIP	18	$4.79 \pm 2.2 \times 10^3$	-14
Type II	287	$7.43\pm^{2.9}_{2.6} \times 10^4$	-14

Table A1 - Table of estimated volumetric rates of a particular SNe types brighter than a particular absolute magnitude with upper and lower 95% confidence intervals given. Also provided are the sample size after selection cuts to give representation of number of supernova involved within the rate calculations. The minimum luminosity to which the calculations were taken to is also provided, with the main focus being type Ia were taken out to -16.5 and Core collapse types were taken out to -14. *The only subtype not included in the calculation for types Ib and Ic was Ib/c as this subtype is not easily distinguishable between the two so would have allowed for bias in either one or both of the rate estimates.

Star Formation Rate Densities from Literature $\log \rho_{SFR}$ $M_{\odot} yr^{-1} Mpc^{-3}$	Derived Supernovae rate densities from Eq [2] $10^5 yr^{-1} Gpc^{-3}$	≈ Ratio between the CCSNe Rate density in this work and that derived from the SFRD in literature	Redshift Range	Agree?	Reference
-1.88 ± 0.04	$0.911 \pm^{0.089}_{0.083}$	1.2	$0 \leq z \leq 0.045$	Yes	Gallego et al (1995)
-1.61 ± 0.10	$1.69 \pm^{0.44}_{0.34}$	0.64	$0 \leq z \leq 0.045$	Yes	Perez-Gonzales et al (2003)
-1.95 ± 0.04	$0.774 \pm^{0.074}_{0.068}$	1.4	$0.01 \leq z \leq 0.12$	No	Nakamura et al (2004)
$-1.80 \pm^{0.13}_{0.08}$	$1.09 \pm^{0.39}_{0.19}$	0.99	$0.001 \leq z \leq 0.017$	Yes	Hanish et al (2006)
-1.80*	1.09	0.99	$0.0 \leq z \leq 0.009$	Yes	James et al (2008)
-1.64*	1.58	0.68	$0.0 \leq z \leq 0.009$	Yes	James et al (2008)
-2.18 ± 0.17	$0.455 \pm^{0.21}_{0.14}$	2.4	$0.01 \leq z \leq 0.10$	No	Westra et al (2010)

Table A2 - Table displaying estimated SFRDs from literature from earlier decades given in logarithmic form and their subsequent conversions to SNeRDs. All but three show agreement or consistency with the CCSNe rate density in this study. The quoted redshift that these studies worked within is given. (Vilella-Rojo, et al., 2020) *No confidence bounds were calculated for this value.

VIII. Acknowledgments

I would like to thank Dr. Dan Perley for his patience and expert guidance and prompt correspondence over the last 6 months of this project. I feel that I have learned a great deal about this area of active research and have gained an incredibly significant interest in continuing to work in this field and on surrounding supernovae demographics. I would also like to thank Christoffer Fremling for providing ***Figure A1*** which was an immense help as it made determining the sky coverage loss factor much smoother and simpler.

Bibliography

Barwick, S. & Beacom, J., 2004. *APS Neutrino Study: Report of the Neutrino Astrophysics and Cosmology Working Group,* College Park: American Physical Society.

Cappellaro, E., Evans, R. & Turatto, M., 1999. A new determination of supernova rates and a comparison with indicators for galactic star formation. *Astronomy and Astrophysics,* Volume 351, pp. 459-466.

Dilday, B. et al., 2010. Measurements of the Rate of Type Ia Supernovae at Redshift lsim0.3 from the Sloan Digital Sky Survey II Supernova Survey. *The Astrophysical Journal,* 713(2), pp. 1026-1036.

Fewell, M. P., 1995. The atomic nuclide with the highest mean binding energy. *American Journal of Physics,* 63(7), pp. 653-658.

Frohmaier, C. et al., 2020. From core collapse to superluminous: the rates of massive stellar explosions from the Palomar Transient Factory. *Monthly Notices of the Royal Astronomical Society,* 500(4), pp. 5142-5158.

Frohmaier, C. et al., 2019. The volumetric rate of normal type Ia supernovae in the local Universe discovered by the Palomar Transient Factory. *Monthly Notices of the Royal Astronomical Society,* 486(2), pp. 2308-2320.

Fryer, C. & New, K., 2003. Gravitational Waves from Gravitational Collapse. *Living Reviews in Relativity,* 6(1).

Gilmore, G., 2004. Astronomy.The short spectacular life of a superstar. *Science(New York, N.Y),* Volume 304, pp. 1915-1916.

Guetta, D. & Della Valle, M., 2007. On the Rates of Gamma-Ray Bursts and Type Ib/c Supernovae. *The Astrophysical Journal,* 657(2), pp. L73-L76.

Hillebrandt, W. & Niemeyer, J. C., 2000. Type Ia Supernova Explosion Models. *Annual Review of Astronomy and Astrophysics,* 38(1), p. 191–230.

Horiuchi, S. et al., 2011. The Cosmic Core-collapse Supernova Rate does not match the Massive-Star Formation Rate. *The Astrophysical Journal,* 738(2), pp. 154-169.

Joseph, T., 2020. *Bootstrapping Statistics. What it is and why it's used..* [Online]
Available at: https://towardsdatascience.com/bootstrapping-statistics-what-it-is-and-why-its-used-e2fa29577307
[Accessed 30 April 2022].

Khokhlov, A., Mueller, E. & Hoeflich, P., 1993. Light curves of type IA supernova models with different explosion mechanisms.. *Astronomy and Astrophysics,* Volume 270, pp. 223-248.

Li, W. et al., 2011. Nearby supernova rates from the Lick Observatory Supernova Search - II. The observed luminosity functions and fractions of supernovae in a complete sample. *Monthly Notices of the Royal Astronomical Society,* 412(3), pp. 1441-1472.

Madau, P. & Dickinson, M., 2014. Cosmic Star Formation History. *Annual Review of Astronomy and Astrophysics,* 52(1), pp. 415-486.

Mazzali, P. A., Röpke, F. K., Benetti, S. & Hillebrandt, W., 2007. A Common Explosion Mechanism for Type Ia Supernovae. *Science,* 315(5813), p. 825–828.

NASA, 2011. *Introduction to Supernova Remnants.* [Online]
Available at: https://heasarc.gsfc.nasa.gov/docs/objects/snrs/snrstext.html
[Accessed 20 February 2022].

Perley, D., 2022. *The ZTF Bright Transient Survey.* [Online]
Available at: https://sites.astro.caltech.edu/ztf/bts/bts.php
[Accessed 15 March 2022].

Perley, D. A., Fremling, C., Sollerman, J. & Miller, A., 2020. The Zwicky Transient Facility Bright Transient Survey. II.A Public Statistical Sample for Exploring Supernova Demographics. *Astrophysical Journal,* 904(1), p. 15.

Röpke, F. K. & Hillebrandt, W., 2004. The case against the progenitor's carbon-to-oxygen ratio as a source of peak luminosity variations in type Ia supernovae. *Astronomy & Astrophysics,* 420(1), p. L1–L4.

Salpeter, E. E., 1955. The Luminosity Function and Stellar Evolution.. *Astrophysical Journal,* Volume 121, p. 161.

Smartt, S., 2009. Progenitors of core-collapse supernovae. *Annual Review of Astronomy and Astrophysics,* 47(1), pp. 63-106.

Taylor, M. et al., 2014. The Core Collapse Supernova Rate from the SDSS-II Supernova Survey. *The Astrophysical Journal,* 792(2), p. 135.

Turatto, M., 2003. Classification of Supernovae. *Lecture Notes in Physics,* pp. 21-36.

Vilella-Rojo, G. et al., 2020. J-PLUS: The star formation main sequence and rate density at d $\lesssim$ 75 Mpc. *Astronomy & Astrophysics,* Volume 650, p. A68.